

UC Berkeley

UC Berkeley Previously Published Works

Title

Disease-associated astrocyte epigenetic memory promotes CNS pathology.

Permalink

<https://escholarship.org/uc/item/9kw9f63r>

Journal

Nature, 627(8005)

Authors

Lee, Hong-Gyun

Rone, Joseph

Li, Zhaorong

et al.

Publication Date

2024-03-01

DOI

10.1038/s41586-024-07187-5

Peer reviewed



HHS Public Access

Author manuscript

Nature. Author manuscript; available in PMC 2025 March 20.

Published in final edited form as:

Nature. 2024 March ; 627(8005): 865–872. doi:10.1038/s41586-024-07187-5.

Disease-associated astrocyte epigenetic memory promotes CNS pathology

Hong-Gyun Lee¹, Joseph M. Rone¹, Zhaorong Li^{1,2}, Camilo Faust Akl¹, Seung Won Shin³, Joon-Hyuk Lee¹, Lucas E. Flausino¹, Florian Pernin⁴, Chun-Cheih Chao¹, Kilian L. Kleemann⁵, Lena Srun¹, Tomer Illouz¹, Federico Giovannoni¹, Marc Charabati¹, Liliana M. Sanmarco¹, Jessica E. Kenison¹, Gavin Piester^{1,6}, Stephanie E. J. Zandee⁷, Jack P. Antel⁴, Veit Rothhammer^{1,8}, Michael A. Wheeler^{1,2}, Alexandre Prat⁷, Iain C. Clark³, Francisco J. Quintana^{1,2,9,✉}

¹Ann Romney Center for Neurologic Diseases, Brigham and Women's Hospital, Harvard Medical School, Boston, MA, USA.

²Broad Institute of MIT and Harvard, Cambridge, MA, USA.

³Department of Bioengineering, College of Engineering, California Institute for Quantitative Biosciences, QB3, University of California Berkeley, Berkeley, CA, USA.

⁴Neuroimmunology Unit, Montreal Neurological Institute, Department of Neurology and Neurosurgery, McGill University, Montreal, Quebec, Canada.

⁵School of Computing, University of Portsmouth, Portsmouth, UK.

⁶Department of Pathology and Laboratory Medicine, University of Rochester Medical Center, Rochester, NY, USA.

⁷Neuroimmunology Research Lab, Centre de Recherche du Centre Hospitalier de l'Université de Montréal (CRCHUM), Montreal, Quebec, Canada.

⁸Department of Neurology, University Hospital, Friedrich-Alexander University Erlangen Nuremberg, Erlangen, Germany.

⁹Gene Lay Institute of Immunology and Inflammation, Boston, MA, USA.

Abstract

Reprints and permissions information is available at <http://www.nature.com/reprints>.

✉ Correspondence and requests for materials should be addressed to Francisco J. Quintana., fquintana@rics.bwh.harvard.edu.

Author contributions H.-G.L., V.R., M.A.W. and F.J.Q. designed the research. H.-G.L., J.M.R., C.F.A., J.-H.L., L.E.F., F.P., C.-C.C., L.S., T.I., F.G., M.C., L.M.S., J.E.K., G.P., S.E.J.Z. and V.R. performed experiments. H.-G.L., Z.L., C.F.A., K.L.K. and F.J.Q. performed bioinformatic analyses. S.W.S. performed FIND-seq. J.P.A., A.P. and I.C.C. provided unique reagents and discussed and/or interpreted findings. H.-G.L. and F.J.Q. wrote the paper with input from coauthors. F.J.Q. directed and supervised the study.

Competing interests The authors declare no competing interests.

Supplementary information The online version contains supplementary material available at <https://doi.org/10.1038/s41586-024-07187-5>.

Springer Nature or its licensor (e.g. a society or other partner) holds exclusive rights to this article under a publishing agreement with the author(s) or other rightsholder(s); author self-archiving of the accepted manuscript version of this article is solely governed by the terms of such publishing agreement and applicable law.

Reporting summary

Further information on research design is available in the Nature Portfolio Reporting Summary linked to this article.

Disease-associated astrocyte subsets contribute to the pathology of neurologic diseases, including multiple sclerosis and experimental autoimmune encephalomyelitis^{1–8} (EAE), an experimental model for multiple sclerosis. However, little is known about the stability of these astrocyte subsets and their ability to integrate past stimulation events. Here we report the identification of an epigenetically controlled memory astrocyte subset that exhibits exacerbated pro-inflammatory responses upon rechallenge. Specifically, using a combination of single-cell RNA sequencing, assay for transposase-accessible chromatin with sequencing, chromatin immunoprecipitation with sequencing, focused interrogation of cells by nucleic acid detection and sequencing, and cell-specific in vivo CRISPR–Cas9-based genetic perturbation studies we established that astrocyte memory is controlled by the metabolic enzyme ATP-citrate lyase (ACLY), which produces acetyl coenzyme A (acetyl-CoA) that is used by histone acetyltransferase p300 to control chromatin accessibility. The number of ACLY⁺p300⁺ memory astrocytes is increased in acute and chronic EAE models, and their genetic inactivation ameliorated EAE. We also detected the pro-inflammatory memory phenotype in human astrocytes in vitro; single-cell RNA sequencing and immunohistochemistry studies detected increased numbers of ACLY⁺p300⁺ astrocytes in chronic multiple sclerosis lesions. In summary, these studies define an epigenetically controlled memory astrocyte subset that promotes CNS pathology in EAE and, potentially, multiple sclerosis. These findings may guide novel therapeutic approaches for multiple sclerosis and other neurologic diseases.

Astrocytes are abundant non-haematopoietic cells of the central nervous system (CNS) that have important functions in health and disease^{9–11}. Astrocytes participate in key processes that are relevant to CNS development and homeostasis⁹. In addition, cytokines, interactions with CNS-resident and CNS-recruited immune cells, and other factors trigger astrocyte responses with important roles in CNS pathology^{10,12,13}. Indeed, several astrocyte subsets have been described in neurologic diseases^{14–16}. For example, we and others have interrogated astrocyte functional heterogeneity in multiple sclerosis and EAE^{1–8}. However, the stability of these disease-associated astrocyte subsets is unclear, an important point when considering lifelong chronic neurologic diseases such as multiple sclerosis.

Immunological memory, the generation of faster and stronger responses upon repeated antigenic stimulation, is a classic hallmark of adaptive immunity driven by long-lived antigen-specific T cells and B cells¹⁷. In addition, innate immune cells including myeloid cells^{18,19} and other cell types^{20,21} undergo metabolic, epigenetic and transcriptional adaptations upon stimulation that alter their subsequent responses, boosting protective immunity against pathogens but also contributing to pathogenic inflammation²². Although memory T cells and B cells have been identified, our understanding of innate immune or non-haematopoietic cell memory subsets remains limited. In this context, it is still unknown whether astrocytes display altered responses to repeated stimulation, how these responses are regulated, and whether specific astrocyte subsets are involved.

Here we describe a memory astrocyte subset controlled by epigenetic changes driven by ACLY- and p300-dependent histone acetylation, which, following an initial stimulation, display faster and stronger pro-inflammatory responses upon restimulation. This subset of memory astrocytes is expanded in EAE and multiple sclerosis, and its genetic inactivation

ameliorates EAE. These findings highlight important mechanisms relevant to the pathology of multiple sclerosis as well as other chronic neurologic disorders and may guide the development of novel therapeutic interventions.

Astrocyte epigenetic memory

To investigate whether an initial pro-inflammatory stimulus affects subsequent astrocyte responses, we administered IL-1 β and TNF (by intracerebroventricular (ICV) injection) to mice once (1 \times IL-1 β + TNF), or twice one week apart (2 \times IL-1 β + TNF); vehicle was used as a control (Fig. 1a). These cytokines were selected because they trigger astrocyte responses similar to those detected in multiple sclerosis and EAE⁷. One day after the last stimulation, we analysed brain astrocytes from the 1 \times and 2 \times treatment groups using RNA sequencing (RNA-seq). On the basis of the number and expression level of differentially expressed genes, 2 \times IL-1 β + TNF stimulation induced more potent pro-inflammatory astrocyte responses than 1 \times IL-1 β + TNF (Fig. 1b–d, Extended Data Fig. 1a,b and Supplementary Table 1).

Ingenuity pathway analysis (IPA) identified NF- κ B as an upstream regulator of the astrocyte response to IL-1 β + TNF; NF- κ B signalling was higher in the 2 \times IL-1 β + TNF group (Fig. 1e). The 2 \times IL-1 β + TNF treatment also increased transcriptional responses linked to histone acetylation, decreasing those linked to histone deacetylase (HDAC) activity (Fig. 1c). Indeed, we also identified *Ep300*, which encodes histone acetyltransferase (HAT) p300, as an upstream regulator of the transcriptional response of astrocytes to 2 \times IL-1 β + TNF stimulation (Fig. 1e and Extended Data Fig. 1c). In support of these findings, the assay for transposase-accessible chromatin with sequencing (ATAC-seq) detected increased chromatin accessibility in inflammation- and epigenetic regulation-related genes following 2 \times IL-1 β + TNF treatment (Fig. 1f,g, Extended Data Fig. 1d,e and Supplementary Table 2). These genes displayed motif enrichment for NF- κ B, ATF-1 and ATF-3, transcription factors that are known to interact with p300 and its paralogue CREB-binding protein^{23,24} (CBP) (Extended Data Fig. 1f).

These in vivo observations may reflect changes in astrocyte-intrinsic responses and/or the control of astrocytes by microglia or other cells^{10,13}. To focus on astrocyte-intrinsic mechanisms, we used primary mouse brain astrocyte cultures. Astrocyte stimulation two times one week apart (2 \times IL-1 β + TNF) boosted genes linked to astrocyte pro-inflammatory activities^{2,8} (*Il6*, *Ccl2* and *Nos2*) and decreased neuronal viability when compared with 1 \times IL-1 β + TNF stimulation (Extended Data Fig. 1g–i). 2 \times IL-1 β + TNF treatment also led to the largest decrease in lactate release (Extended Data Fig. 1j), suggestive of a stronger impairment in astrocyte support of neuron metabolic needs²⁵. Of note, astrocyte pro-inflammatory gene expression induced by IL-1 β + TNF stimulation in vitro returned to basal levels 7 days after the initial cytokine stimulation (Extended Data Fig. 1k).

Increased astrocyte responsiveness following in vitro 2 \times IL-1 β + TNF stimulation may reflect altered cell-intrinsic responses in previously activated astrocytes and/or the engagement of astrocytes not activated in the first activation round. To study cell-intrinsic responses in previously activated astrocytes, we used primary mouse brain astrocytes from

p65-eGFP (specifically *Rela*-eGFP) reporter mice. In these astrocyte cultures, IL-1 β + TNF stimulation induced p65-driven eGFP expression (Extended Data Fig. 1i); 2 \times IL-1 β + TNF stimulation triggered higher NF- κ B activation than 1 \times IL-1 β + TNF. Thus, we sorted eGFP⁺ and eGFP⁻ astrocytes by fluorescence-activated cell sorting (FACS) following one round of IL-1 β + TNF stimulation, and after a resting period of 7 days, we restimulated sorted astrocytes with IL-1 β + TNF (Fig. 1h and Extended Data Fig. 1m). Note that both eGFP and pro-inflammatory gene expression returned to basal levels 7 days after the first IL-1 β + TNF stimulation (Extended Data Fig. 1n,o). We detected higher *Il6*, *Ccl2* and *Nos2* expression and stronger NF- κ B activation upon restimulation in eGFP⁺ versus eGFP⁻ sorted astrocytes (Fig. 1i and Extended Data Fig. 1p). These findings suggest that cell-intrinsic mechanisms alter the subsequent response of astrocytes to stimulation.

Our RNA-seq and ATAC-seq analyses detected increased signatures linked to histone acetylation in the 2 \times IL-1 β + TNF treatment group (Fig. 1c and Extended Data Fig. 1c,f), identifying the HATs p300, Tip60 and PCAF as candidate regulators (Extended Data Figs. 1c and 2a). However, in primary mouse astrocytes, 2 \times IL-1 β + TNF activation in vitro increased *Ep300*, but not *Kat5* (also known as *Tip60*) or *Kat2b* (also known as *Pcaf*) expression; increased *Ep300* expression persisted upon 3 \times IL-1 β + TNF stimulation (Extended Data Fig. 2b,c). Indeed, the p300 inhibitor C646 suppressed the increase in *Il6*, *Ccl2* and *Nos2* expression induced by 2 \times IL-1 β + TNF (Extended Data Fig. 2d,e). Of note, p300 pharmacological inactivation did not alter NF- κ B activation following 1 \times IL-1 β + TNF stimulation, but abrogated the increased expression of *Il6*, *Ccl2* and *Nos2* induced in eGFP⁺ *p65*-eGFP astrocytes by 2 \times IL-1 β + TNF stimulation (Fig. 1j and Extended Data Figs. 2f,g). Together, these findings suggest that p300-driven epigenetic memory boosts astrocyte pro-inflammatory responses following an initial pro-inflammatory stimulation.

p300 drives astrocyte epigenetic memory

Astrocytes have important roles in multiple sclerosis and EAE pathology¹⁻⁸. To study the relevance of astrocyte epigenetic memory in vivo, we first generated a transcriptional signature score based on the response to 2 \times IL-1 β + TNF treatment detected by RNA-seq (Fig. 1a, Extended Data Fig. 3a and Supplementary Table 3). The analysis of our single-cell RNA sequencing (scRNA-seq) datasets² detected an increased transcriptional signature score linked to epigenetic memory-driven astrocytes at EAE peak (Extended Data Fig. 3b). Indeed, ICV IL-1 β + TNF stimulation of brain astrocytes isolated 22 days after EAE induction induced higher *Il6*, *Ccl2* and *Nos2* expression than in naive mice, which resembled the increased responses detected in vitro following 2 \times IL-1 β + TNF (Extended Data Figs. 2c-e).

We identified p300 as a candidate regulator of astrocyte epigenetic memory (Fig. 1j and Extended Data Figs. 1c,f and 2e); p300 controls histone 3 acetylation at lysine 27 (H3K27ac). Indeed, we detected an increase in p300⁺ and H3K27ac⁺p300⁺ astrocytes in spinal cord white matter during EAE (Fig. 2a). To study the role of p300 in astrocytes during EAE, we inactivated *Ep300* using a *Gfap* promoter-driven CRISPR-Cas9 lentiviral vector, as previously described^{1-4,6,7}. *Ep300* inactivation ameliorated EAE and suppressed pro-inflammatory astrocyte responses as determined by RNA-seq, but did not affect

CNS-recruited or peripheral CD4⁺ T cells (Fig. 2b–d, Extended Data Fig. 3f–k and Supplementary Table 4). *Ep300* inactivation also suppressed transcriptional signatures linked to epigenetic memory astrocytes, NF- κ B and H3K27ac (Fig. 2c,d and Extended Data Fig. 3f,h). In support of these findings, chromatin immunoprecipitation followed by sequencing (ChIP–seq) detected decreased H3K27ac marks in genes related to metabolism, NF- κ B signalling, and inflammation following *Ep300* inactivation in astrocytes (Figs. 2e–g, Extended Data Fig. 3l and Supplementary Table 5). Further support for a role of p300 in astrocyte epigenetic memory was provided by the analysis of primary mouse brain astrocytes in culture, where 2 \times IL-1 β + TNF boosted p300 recruitment to *Il6*, *Ccl2* and *Nos2* promoters (Extended Data Fig. 3m). Collectively, these findings suggest that p300-driven histone acetylation regulates pro-inflammatory epigenetic memory astrocyte responses.

ACLY controls p300-driven epigenetic memory

HATs acetylate histone lysine residues using acetyl-CoA as a substrate²⁶. Acetyl-CoA used for histone acetylation is generated by two major enzymes in mammals: ATP-citrate lyase (ACLY) and acetyl-CoA synthetase 2 (ACSS2), which use citrate and acetate as substrates, respectively^{26,27}. To define the enzymatic source of acetyl-CoA involved in the control of astrocyte epigenetic memory, we first analysed mouse brain astrocytes stimulated in vitro with 1 \times or 2 \times IL-1 β + TNF, finding that astrocyte restimulation boosts *Acly* but not *Acss2* expression (Extended Data Fig. 4a). Indeed, *Acly* expression persisted upon additional IL-1 β + TNF stimulation (3 \times), recapitulating our findings on *Ep300* expression (Extended Data Figs. 2c and 4b). Moreover, in immunohistochemistry (IHC) studies, we detected increased numbers of ACLY⁺ astrocytes in spinal cord white matter during EAE (Extended Data Fig. 4c,d), suggesting a role for ACLY in the control of astrocyte epigenetic memory; ACSS2⁺ astrocytes were decreased in EAE.

To evaluate the functional relevance of these findings, we inactivated *Acly* or *Acss2* in CNS astrocytes using a *Gfap*-driven CRISPR–Cas9 lentivirus-based approach. The inactivation of *Acly*, but not *Acss2*, ameliorated EAE (Fig. 3a and Extended Data Fig. 5a), decreasing the expression of transcriptional modules linked to astrocyte epigenetic memory, inflammation, and NF- κ B signalling (Fig. 3b–d and Supplementary Table 6), but did not affect the number of CNS or peripheral CD4⁺ T cells (Extended Data Fig. 5c–e). Astrocyte *Acly* inactivation also suppressed demyelination and decreased transcriptional programmes linked to acetyl-CoA biosynthesis and H3K27 acetylation (Fig. 3d and Extended Data Fig. 5a,b). Indeed, we detected decreased H3K27ac marks in *Il6* and *Ccl2* promoters following *Acly* inactivation (Fig. 3e). In addition, astrocyte *Acly* inactivation down-regulated p300-driven NF- κ B signalling during EAE (Fig. 3f and Supplementary Table 7). Finally, in support for a role of ACLY in p300 activation in astrocytes during CNS inflammation, we detected an increase in ACLY⁺ p300⁺ astrocytes in spinal cord white matter during EAE (Fig. 3g and Extended Data Fig. 5f).

To validate these findings, we used the EAE model induced in NOD mice by immunization with the peptide MOG_{35–55}, which recapitulates some aspects of secondary progressive multiple sclerosis^{8,28}. First, we confirmed that ICV administration of IL-1 β + TNF in NOD EAE mice 124 days after disease induction (during the progressive disease phase) induced

higher brain astrocyte *Il6*, *Ccl2* and *Nos2* expression than in naive mice (Extended Data Figs. 6a–c). Moreover, we detected increased H3K27ac⁺p300⁺ and ACLY⁺p300⁺ astrocytes in spinal cord white matter during EAE in NOD mice (Extended Data Fig. 6d,e). Finally, *Acly* or *Ep300* lentivirus-driven inactivation in astrocytes suppressed EAE progression in NOD mice, reduced demyelination and decreased astrocyte transcriptional responses linked to H3K27 acetylation, epigenetic memory, NF- κ B signalling and inflammation, as determined by IHC and RNA-seq; no significant changes were detected in CNS or peripheral CD4⁺ T cells (Extended Data Figs. 6f–i and 7a–e and Supplementary Table 8). Together, these findings demonstrate that ACLY–p300-driven epigenetic memory in astrocytes promotes CNS pathology.

FIND-seq analysis of ACLY⁺EP300⁺ astrocytes

Our studies identified a subset of ACLY⁺p300⁺ astrocytes that promote EAE pathology, but the intracellular localization of ACLY and p300 limits their use to isolate and study in-depth ACLY⁺p300⁺ astrocytes. To enable genome-wide transcriptional analyses of cells of interest defined by mRNA or DNA markers, we developed focused interrogation of cells by nucleic acid detection and sequencing²⁹ (FIND-seq) to analyse *Acly*⁺*Ep300*⁺ astrocytes.

First, we used FIND-seq to analyse *Acly*[−]*Ep300*[−], *Acly*⁺*Ep300*[−], *Acly*[−]*Ep300*⁺ and *Acly*⁺*Ep300*⁺ astrocytes isolated from the CNS of TdTomato^{*Gfap*} mice (Fig. 4a,b and Extended Data Fig. 8a–f). In agreement with our previous IHC analyses, there were increased numbers of *Acly*⁺*Ep300*⁺ astrocytes in EAE (Fig. 4b). Moreover, the transcriptional profile of *Acly*⁺*Ep300*⁺ astrocytes from EAE mice was closely correlated with the transcriptional signature of epigenetic memory defined based on the analysis of astrocytes following 2× IL-1 β + TNF treatment in vivo; *Acly*[−]*Ep300*⁺ and *Acly*⁺*Ep300*[−] astrocyte subsets displayed intermediate profiles of this signature, suggesting that they represent transitional states towards the establishment of astrocyte epigenetic memory (Fig. 4c and Extended Data Fig. 8g).

Next, to interrogate the heterogeneity of memory astrocytes in autoimmune CNS inflammation, we re-analysed our astrocyte EAE scRNA-seq dataset generated in TdTomato^{*Gfap*} mice². Using the transcriptional signature of *Acly*⁺*Ep300*⁺ EAE astrocytes (Supplementary Table 9), we identified an astrocyte subset (cluster 3) that expanded 18.3-fold in EAE (Fig. 4d–g, Extended Data Fig. 8h and Supplementary Table 10). Indeed, the transcriptional signature of astrocytes in cluster 3 was the one most closely correlated with the transcriptional signature of astrocytes following 2× IL-1 β + TNF treatment in vivo (Fig. 4f). Astrocytes in cluster 3 displayed the activation of pro-inflammatory pathways linked to astrocyte pathogenic activities and increased NF- κ B signalling controlled by ACLY–p300-dependent epigenetic regulation (Fig. 4h,i and Supplementary Table 11). Moreover, a pseudotime analysis revealed a gradual transition toward cluster 3 astrocytes associated with epigenetic memory, which displayed a transcriptional profile enriched for genes linked to inflammation and NF- κ B signalling (Fig. 4j,k). Notably, clusters 1 and 10 correspond to pathogenic astrocyte subsets expanded in EAE, which represent candidate intermediate states for the development of astrocyte pro-inflammatory memory controlled by p300-dependent NF- κ B signalling (Fig. 4e–g and Extended Data Fig. 8i–l). Thus,

FIND-seq identified a disease-associated memory astrocyte subset controlled by ACLY- and p300-dependent epigenetic marks which promotes CNS inflammation.

Astrocyte epigenetic memory in multiple sclerosis

Astrocytes contribute to multiple sclerosis pathology^{10,13}. We therefore investigated whether pro-inflammatory astrocyte epigenetic memory responses can be induced in human astrocytes. Human fetal astrocytes in culture displayed increased pro-inflammatory responses following 2× IL-1β + TNF stimulation, which were abrogated by treatment with the p300 inhibitor C646 (Extended Data Fig. 9a).

We next integrated two independent scRNA-seq datasets^{30,31}, generating a dataset of 16,276 astrocytes from 17 patients with multiple sclerosis and 12 controls. Unbiased clustering identified 6 astrocyte clusters in multiple sclerosis (Fig. 5a, Extended Data Fig. 9b–e and Supplementary Tables 12 and 13). Consistent with our EAE scRNA-seq studies (Fig. 4d–i), we identified an astrocyte subset (cluster 2) that was expanded 24.5-fold in multiple sclerosis chronic lesions (20.4-fold in chronic active lesions and 4.1-fold in chronic inactive lesions), which displayed a transcriptional signature similar to the one in mouse *Acly*⁺*Ep300*⁺ astrocytes (Fig. 5a–c and Extended Data Fig. 9f,g). This astrocyte subset displayed increased pro-inflammatory and NF-κB signalling (Fig. 5d,e). Indeed, IPA identified ACLY–p300 signalling as an upstream regulator of NF-κB in cluster 2 astrocytes (Fig. 5f and Supplementary Table 14). Furthermore, pseudotime analysis revealed a transitional memory state towards cluster 2 astrocytes, which displayed a transcriptional profile enriched for genes related to histone acetylation, inflammation and NF-κB signalling (Fig. 5g,h).

Finally, to validate these findings we analysed multiple sclerosis and control CNS samples by IHC. In agreement with our scRNA-seq analyses, we detected an increase in nuclear ACLY⁺p300⁺ astrocytes in multiple sclerosis white matter lesions compared with control samples (Fig. 5i and Extended Data Fig. 10a). These findings define a potential role of ACLY–p300-driven pro-inflammatory astrocyte epigenetic memory in multiple sclerosis pathology.

Discussion

Here we describe ACLY⁺p300⁺ memory astrocytes that promote CNS pathology. Previous reports have described long-lived epigenetic memory in innate immune cells and their progenitors^{18,21,32,33}. Our findings suggest that astrocytes—non-haematopoietic CNS cells—also exhibit epigenetic memory. Considering the long lifespan and low turnover rate of astrocytes^{34,35}, astrocyte epigenetic memory may have important roles in the pathology of chronic neurologic disorders.

p300 and its paralogue CBP regulate transcriptional programmes via the acetylation of histones and other proteins³⁶. The brain displays the highest p300 and CBP HAT activity in the body³⁷. Indeed, histone acetylation and other post-translational modifications, have been linked to long-term memory, including recognition and contextual fear^{37–40}. p300 also regulates cellular senescence and stress response, which promote systemic chronic

inflammation^{24,41–43}. However, little is known about the role of p300 and CBP in CNS inflammation and neurodegeneration. Of note, a recent comparative study detected p300 upregulation in astrocytes in multiple pro-inflammatory contexts⁴⁴, suggesting that p300-driven astrocyte epigenetic programmes contribute to the pathogenesis of multiple neurologic conditions. In addition, p300 interacts with multiple partners including NF- κ B²³; a central regulator of pathogenic astrocyte responses^{10,13}. Indeed, NF- κ B acetylation boosts pro-inflammatory transcriptional responses⁴⁵. In this context, our findings suggest that p300-dependent histone acetylation boosts NF- κ B-driven pro-inflammatory transcriptional responses in astrocytes. This increased activation of NF- κ B-driven transcriptional modules may reflect both the increased accessibility to NF- κ B responsive DNA elements, as well as the heightened recruitment of NF- κ B via protein–protein interactions, boosting pathogenic activities in memory astrocytes.

Metabolic adaptations are integrated into epigenetic marks to control transcriptional responses^{22,46}. Indeed, nuclear acetyl-CoA levels control HAT activity²⁶. For example, chromatin-recruited ACSS2 regulates CBP-mediated histone acetylation in hippocampal neurons during memory formation⁴⁰. Our studies suggest that the metabolic remodelling induced in astrocytes by pro-inflammatory cytokines⁸ is linked to ACLY-driven acetyl-CoA production, highlighting how inflammation-induced metabolic adaptation in astrocytes amplifies astrocyte pro-inflammatory responses. These findings resemble previous observations on how inflammation-triggered changes in sphingolipid metabolism boost NF- κ B driven astrocyte pro-inflammatory responses^{8,28}.

ACLY is expressed by neurons and glial cells in the CNS⁴⁷. ACLY-produced acetyl-CoA, is used as an acetyl group donor by p300 during histone acetylation²⁷. ACLY also controls T cell and macrophage responses^{48–50}, highlighting common mechanisms that regulate the pro-inflammatory responses of haematopoietic and non-haematopoietic cells such as astrocytes. Indeed, although we focused on astrocyte-intrinsic mechanisms of epigenetic memory, interactions with other cells in the CNS such as microglia are also likely to modulate astrocyte epigenetic memory^{10,13}. Astrocytes also establish regulatory interactions with peripheral immune cells recruited to the CNS^{2,3,6}. Finally, recent reports suggest that neurons modulate astrocyte responses via the regulation of histone serotonylation⁵¹. Thus, cell–cell interactions with CNS-resident and CNS-recruited cells may integrate multiple stimuli to regulate astrocyte epigenetic memory.

In summary, we identified epigenetically controlled ACLY⁺p300⁺ memory astrocytes that promote CNS pathology in autoimmune inflammation. These findings constitute an example of mechanisms of structural immunity⁵², pro-inflammatory pathogenic responses induced in tissue-resident non-haematopoietic cells in response to interactions with CNS-resident and CNS-recruited immune cells. Indeed, ACLY⁺p300⁺ memory astrocytes were most expanded in CNS chronic active lesions that were linked to multiple sclerosis progression³⁰. Recent developments in the understanding of the mechanism of action of ACLY have guided the development of specific inhibitors for the treatment of cancer and metabolic conditions^{53–55}. These ACLY inhibitors may be repurposed for the therapeutic modulation of ACLY⁺p300⁺ memory astrocytes in multiple sclerosis and other neurologic disorders.

Online content

Any methods, additional references, Nature Portfolio reporting summaries, source data, extended data, supplementary information, acknowledgements, peer review information; details of author contributions and competing interests; and statements of data and code availability are available at <https://doi.org/10.1038/s41586-024-07187-5>.

Methods

Mice

Adult male and female mice, and postnatal pups were used on a C57BL/6 J background (000664, The Jackson Laboratory); NOD/ShiLtJ (001976, The Jackson Laboratory) mice were obtained from the Jackson Laboratory. B6.Cg-Tg(Gfap-cre)^{73.12Mvs/J} mice⁵⁶ (The Jackson Laboratory, 012886) mice were crossed with B6.Cg-Gt(ROSA)^{26Sort}m9(CAG-tdTomato)Hze/J mice⁵⁷ (The Jackson Laboratory, 007909) to generate *Gfap*^{cre/+}; *TdTomato*^{fl/+} (*TdTomato*^{Gfap}) mice. Postnatal pups were used from the NF-κB reporter strain FVB.Cg-Tg(HIV-eGFP,luc)^{8Tsb/J}⁵⁸ (The Jackson Laboratory, 027529) at postnatal day (P)0–P3. Mice were kept in a pathogen-free facility at the Hale Building for Transformative Medicine at Brigham and Women's Hospital in accordance with the IACUC guidelines. 9–12-week-old mice were used for stereotactic injection and EAE induction. Pups were euthanized between P0 and P3 for collection and culturing astrocytes. All procedures were reviewed and approved under the IACUC guidelines at Brigham and Women's Hospital.

In vivo cytokine stimulation

C57BL/6 J mice at age 10–12 weeks were anaesthetized using 1–3% isoflurane mixed with oxygen. Heads were shaved and cleaned using 70% ethanol and Betadine (Thermo Fisher, 19-027132) followed by a medial incision of the skin to expose the skull. Mice were injected with 100 ng ml⁻¹ IL-1β (R&D Systems, 401-ML-005, 100 μg ml⁻¹ stock in PBS) and 50 ng ml⁻¹ TNF (R&D Systems, 410-MT-010, 100 μg ml⁻¹ stock in PBS) diluted in PBS or PBS. At day 7, mice were re-injected (2×) or injected (1×) with 100 ng ml⁻¹ IL-1β and 50 ng ml⁻¹ TNF or PBS for 18–24 h and astrocytes were sorted for further analysis. For EAE experiments, mice were injected with 100 ng ml⁻¹ IL-1β and 50 ng ml⁻¹ TNF or PBS for 18–24 h and astrocytes were sorted for further analysis. The lateral ventricles were targeted bilaterally using the coordinates: ±1.0 (lateral), -0.44 (posterior), -2.2 (ventral) relative to bregma. Mice were injected by two 5 μl injections using a 25 μl Hamilton syringe (Sigma-Aldrich, 20787) on a stereotaxic alignment system (Kopf, 1900) and the incision was sutured.

Primary astrocyte cultures from neonatal mice

Procedures were performed as described previously⁵⁹. Brains of mice aged P0–P3 were dissected into PBS on ice. Cortices were discarded and the brain parenchyma were pooled, centrifuged at 500g for 10 min at 4 °C and resuspended in 0.25% Trypsin-EDTA (Thermo Fisher Scientific, 25200-072) at 37 °C for 10 min. Trypsin was neutralized by adding DMEM (Thermo Fisher Scientific, 11965118) supplemented with 10% FBS (Thermo Fisher

Scientific, 10438026) and 1% penicillin/streptomycin (Thermo Fisher Scientific, 15140148), and cells were passed through a 70- μm cell strainer. Cells were centrifuged at 500g for 10 min at 4 °C, resuspended in DMEM with 10% FBS/1% penicillin/streptomycin and cultured in T-75 flasks (Falcon, 353136) at 37 °C in a humidified incubator with 5% CO₂, for 7–10 days until confluency was reached. Astrocytes were shaken for 30 min at 180 rpm, the supernatant was collected for microglia and the media was changed, then astrocytes were shaken for at least 2 h at 220 rpm and the supernatant was aspirated and the media was changed again. Medium was replaced every 2–3 days. Primary astrocytes were treated with 100 ng ml⁻¹ IL-1 β (R&D Systems, 401-ML-005, 100 μg ml⁻¹ stock in PBS) and 50 ng ml⁻¹ TNF (R&D Systems, 410-MT-010, 100 μg ml⁻¹ stock in PBS) diluted in DMEM (Thermo Fisher Scientific, 11965118) that was supplemented with 10% FBS (Life Technologies, 10438026) and 1% penicillin/streptomycin (Life Technologies, 15140122) or PBS. The medium was replaced and washed twice after 18–24 h, then astrocytes were rested for 6 days. Medium was replaced every 2–3 days. At day 7, astrocytes were re-treated (2 \times) or treated (1 \times) with 100 ng ml⁻¹ IL-1 β and 50 ng ml⁻¹ TNF or PBS for 30 min. Astrocytes were stimulated and collected on day 14 for 3 \times treatment. For p65 sorting experiments, eGFP⁺ and eGFP⁻ astrocytes were FACS sorted after 18–24 h of IL-1 β and TNF treatment and re-seeded and rested for 6 days. Astrocytes were subsequently gated on: CD11b⁻CD45⁻EGFP^{+/-}. Medium was replaced every 2–3 days. At day 7, astrocytes were re-treated (2 \times) or treated (1 \times) with 100 ng ml⁻¹ IL-1 β and 50 ng ml⁻¹ TNF or PBS for different time points (5 min to 1 h). Inhibitor compound treatment was pre-treated at 37 °C for 2 h before the first cytokine treatment, then co-treated with IL-1 β and TNF for 18–24 h. The inhibitors used in these studies are: 5 μM C646 (Selleck Chemicals, S7152), 5 μM MB-3 (Sigma-Aldrich, M2449), and 5 μM MG149 (Medchem Express, HY-15887).

Neuronal viability assay

Ten-thousand N2A neuronal cells (ATCC, CCL-131) were plated in each well of 96-well plates and preactivated with 100 ng ml⁻¹ mouse IFN γ (R&D Systems, 485-MI-100) for 18–24 h. Thereafter, medium was replaced after extensive washing with 1 \times PBS, adding 200 μl of astrocyte-conditioned medium per well. Eighteen to twenty-four hours later, the supernatant was collected for cytotoxicity evaluation by measuring LDH release with CytoTox 96 nonradioactive cytotoxicity assay kit (Promega, G1780), following the protocol suggested by the manufacturer.

Lactate release measurement

Two days after seeding on 48-well plate, 200,000 astrocytes were cultured in 1 mM glucose DMEM medium (A1443001, GIBCO) supplied 100 unit ml⁻¹ penicillin/streptomycin without FBS for at least 48 h. Thereafter, medium was removed, cells washed with 1 \times PBS, treated with 100 ng ml⁻¹ IL-1 β (R&D Systems, 401-ML-005, 100 μg ml⁻¹ stock in PBS) and 50 ng ml⁻¹ TNF (R&D Systems, 410-MT-010, 100 μg ml⁻¹ stock in PBS) diluted in DMEM (Thermo Fisher Scientific, 11965118) that was supplemented with 10% FBS (Life Technologies, 10438026) and 1% penicillin/streptomycin (Life Technologies, 15140122) or PBS. The medium was replaced after 18–24 h, then astrocytes were rested for 6 days. Medium was replaced every 2–3 days. At day 7, astrocytes were re-treated (2 \times) or treated (1 \times) with 100 ng ml⁻¹ IL-1 β and 50 ng ml⁻¹ TNF or PBS for 1 h. The

medium was collected for filtration with Amicon Ultracel 10k (Millipore, UFC501096) under 12,000g centrifuge at 4 °C for 30 min. Lactate in flow-through medium was quantified using the l-lactate assay kit (Biomedical Research Service and Clinical Application, A-108) and GloMax microplate reader (Promega) as suggested by the manufacturer. The absorption signal was normalized to cell number estimated using CyQUANT cell proliferation assay kit (Invitrogen, C7026) first and then compared to control group for data analysis.

Immunostaining of mouse CNS tissue

Mice were intracardially perfused with ice cold 1× PBS and a 0.5-cm section of the superior spinal column was excised from the mouse then post-fixed in 4% PFA overnight at 4 °C. Following fixation, the vertebral column was de-calcified with 20% EDTA (pH 7.4) for 1 week at 4 °C with inversion, then the tissue was dehydrated with 30% sucrose for one week at 4 °C. Spinal cords were frozen in OCT (Sakura, 4583) and 8–20 μm sections were prepared by cryostat on SuperFrost Plus Gold slides (Fisher Scientific, 15-188-48). Sections were permeabilized with 1× permeabilization buffer (BD Biosciences, 554723) for 10 min at room temperature, then blocked using serum-free protein block (Agilent, X0909) for 10 min at room temperature. Sections were then incubated with primary antibodies diluted in 1× permeabilization buffer overnight at 4 °C. Following primary antibody incubation, sections were washed 3× with 1× permeabilization buffer and incubated with secondary or conjugated antibodies diluted in 1× permeabilization buffer for 1 h at room temperature. After secondary and conjugated antibody incubation, sections were stained with 1 μg ml⁻¹ DAPI (Sigma-Aldrich, D9542) diluted in 1× permeabilization buffer for 5 min at room temperature, then washed 3× with 1× permeabilization buffer and mounted with ProLong Gold Antifade Mountant (Fisher Scientific, P36930). Iterative labelling using rabbit primary antibodies was accomplished by incubating with a single primary antibody on day 1, staining with the anti-rabbit Fab 568 fragment on day 2, washing 6× with 1× permeabilization buffer, followed by incubation with primary and secondary antibodies as described above. Primary antibodies used in this study were: rabbit anti-p300 (Cell Signaling Technology, 1:50, 70088S), rabbit anti-ACLY (ProteinTech Group, 1:100, 15421-1-AP), rabbit anti-H3K27ac (Abcam, 1:100, ab4729) and goat anti-SOX9 (R&D Systems, 1:100, AF3075). Secondary antibodies used in this study were: Rhodamine Red-X-AffiniPure Fab Fragment donkey anti-rabbit IgG (H + L) (Jackson ImmunoResearch, 711-297-003) and Alexa Fluor 647 AffiniPure Fab Fragment donkey anti-rabbit IgG (H + L) (Jackson ImmunoResearch, 711-606-152) both at 1:1,000 working dilution. The conjugated antibody used in this study was mouse anti-GFAP Alexa Fluor 488 (GA5) (Fisher Scientific, 1:100, 53-9892-82). For FluoroMyelin Fluorescent Myelin staining, sections were permeabilized and blocked with 4% Bovine Serum Albumin (BSA, Sigma, A3294), 0.3% Triton X-100 (Sigma, T8787) in 1× PBS for 1 h at room temperature. To label the myelinated area, Fluoromyelin dye (Thermo Fisher Scientific, 1:300, F34652) were stained in 1× permeabilization buffer (BD Biosciences, 554723) for 30 min at room temperature. Stained spinal cord tissues were washed 3× with 1× permeabilization buffer and mounted with ProLong Gold Antifade Mountant. Sections were imaged were stitched on an LSM-880-AiryScan confocal microscope using the ZEN Black software (Zeiss), and image analysis was performed with FIJI version of ImageJ (NIH).

Immunostaining of CNS tissue from multiple sclerosis patients

For immunostaining of paraffin sections, sections were deparaffinized in 2× washes of Xylenes for 10 min (Sigma-Aldrich, 214736), followed by 2× washes in 100% ethanol for 10 min, 1× wash in 95% ethanol for 5 min, 1× wash in 70% ethanol for 5 min, 1× wash in 50% ethanol for 5 min, and then slides were rinsed with ddH₂O for 5 min. Antigen retrieval was performed by placing slides in boiling Epitope Retrieval Solution (IHC World, IW-11000) for 20 min. Slides were dried, a hydrophobic barrier was made (Vector Laboratories, H-4000) and sections were washed 3× for 5 min with 0.3% Triton X-100 in PBS (PBS-T). Sections were blocked with 5% donkey serum (Sigma-Aldrich, D9663) in 0.3% PBS-T at room temperature for 30 min. Sections were then incubated with primary antibody diluted in blocking buffer overnight at 4 °C. Following primary antibody incubation, sections were washed 3× with 0.3% PBS-T and incubated with secondary antibody diluted in blocking buffer for 2 h at room temperature. Sections were then washed 3× with 0.3% PBS-T, dried, and coverslips were mounted. Iterative labelling using rabbit primary antibodies was accomplished by incubating with a single primary antibody on day 1, staining with the anti-rabbit Fab 568 fragment on day 2, washing 6× with 1× permeabilization buffer, followed by incubation with primary and secondary antibodies as described above. Primary antibodies used in this study were: rabbit anti-P300 (Cell Signaling Technology, 1:50, 70088 S), rabbit anti-ACLY (ProteinTech Group, 1:100, 15421-1-AP) and goat anti-SOX9 (R&D Systems, 1:100, AF3075). Secondary antibodies used in this study were: Rhodamine Red-X-AffiniPure Fab Fragment donkey anti-rabbit IgG (H + L) (Jackson ImmunoResearch, 711-297-003) and Alexa Fluor 647 AffiniPure Fab Fragment donkey anti-rabbit IgG (H + L) (Jackson ImmunoResearch, 711-606-152) both at 1:1,000 working dilution. The conjugated antibody used in this study was mouse anti-GFAP Alexa Fluor 488 (GA5) (Fisher Scientific, 1:100, 53-9892-82). Human brain tissue was obtained from patients diagnosed with clinical and neuropathological multiple sclerosis diagnosis according to the revised 2017 McDonald's criteria⁶⁰. Tissue samples were collected from healthy donors and multiple sclerosis patients with full ethical approval and informed consent as approved by the local ethics committee from the Centre de Recherche du Centre Hospitalier de l'Université de Montréal (CRCHUM) under ethical approval number BH07.001, Nagano 20.332-YP. Autopsy samples were preserved, and lesions classified using luxol fast blue and haematoxylin and eosin staining as previously published^{61,62}.

Unbiased immunofluorescence quantification

Astrocyte H3K27ac, ACLY, and p300 expression were quantified as previously described^{63,64}. In brief, GFAP-positive cells were detected by implementing the bwlabel algorithm for labeling connected components in 2D images using MATLAB (MathWorks). Small puncta sized <50 μm² were regarded as artefacts and were filtered out. Blood vessel related fluorescence artefacts were manually removed. Next, the averaged H3K27ac, ACLY, and p300 fluorescence intensities were calculated per individual GFAP-positive cells and outliers were removed using the Robust Regression and Outlier Removal (ROUT) method⁶⁵ with coefficient $Q = 1\%$.

CRISPR–Cas9 lentivirus production

Lentiviral constructs were generated by modifying the pLenti-U6-sgScramble-Gfp-Cas9-2A-eGFP-WPRE lentiviral backbone, described previously⁴. This backbone contains derivatives of the previously described reagents lentiCRISPR v2 (a gift from F. Zhang, Addgene plasmid #52961⁶⁶), and lentiCas9-eGFP (a gift from P. Sharp and F. Zhang, Addgene plasmid #63592⁶⁷). The *Gfp* promoter is the ABC₁D *gfa2* *GFAP* promoter⁶⁸. Substitution of sgRNAs was performed through a PCR-based cloning strategy using Phusion Flash HF 2× Master Mix (Thermo Fisher, F548L). A three-way cloning strategy was developed to substitute sgRNAs using the following primers: U6-PCR-F 5′-AAAGGCGCGCCGAGGGCCTATTT-3′, U6-PCR-R 5′-TTTTTTGGTCTCCCGGTGTTTCGTCCTTTCCAC-3′, cr-RNA-R 5′-GTTCCCTGCAGGAAAAAAGCACCGA-3′, cr-RNA-F 5′-AAAAAAGGTCTCTACCG(N₂₀)GTTTTAGAGCTAGAAATAGCAAGTT-3′, where N₂₀ marks the sgRNA substitution site. The following sgRNA were designed using a combination of the Broad GPP sgRNA Designer Webtool (Spyo-Cas9, <http://portals.broadinstitute.org/gpp/public/analysis-tools/sgrna-design>), Synthego (<https://design.synthego.com/#/>), and cross-referenced with activity-optimized sequences contained within the Addgene library #1000000096 (a gift from D. Sabatini and E. Lander)⁶⁹. The sgRNA sequences used are as follows, with the promoter indicated in parentheses: sgScrambl - 5′-GCACTACCAGAGCTAACTCA-3′, sg*Ep300* - 5′-ACAGAATTGGGACTAACCAA-3′, sg*Acly* - 5′-GAGAGA GATTGACCCCGACG-3′, sg*Acss2* - 5′-GTTTTGGGGAAACATTGCCA-3′. Amplicons were purified using the QIAquick PCR Purification Kit (Qiagen, 28104) and digested using DpnI (NEB, R0176S), BsaI-HF (NEB, R3535/R3733), AscI (for U6 fragment) (NEB, R0558), or SbfI-HF (for crRNA fragment) (NEB, R3642). pLenti backbone was cut with AscI/SbfI-HF and purified using the QIAquick PCR purification kit. Ligations into the respective backbone were performed overnight at 16 °C using T4 DNA Ligase Kit (NEB, M0202L). Ligations were transformed into NEB Stable *Escherichia coli* (NEB, C3040) at 42 °C and the ligation products were spread onto ampicillin selection plates. After overnight incubation at 37 °C, single colonies were picked and DNA was prepared using QIAprep spin miniprep kit (Qiagen, 27104). Lentiviral plasmids were transfected into HEK293FT cells according to the ViraPower Lentiviral Packaging Mix protocol (Thermo Fisher Scientific, K497500) and lentiviruses were packaged with pLP1, pLP2, and pseudotyped with pLP/VSVG. Supernatant was aspirated the following day and fresh medium was added. After 2 days of incubation, lentivirus was collected and concentrated using Lenti-X Concentrator (Clontech, 631231) overnight at 4 °C followed by centrifugation according to the manufacturer's protocol. Lentiviral pellets were resuspended in 1/500 of the original volume and stored at –80 °C.

Intracranial lentivirus injection

C57Bl/6 J mice at age 10–12 weeks were anaesthetized using 1–3% isoflurane mixed with oxygen. Heads were shaved and cleaned using 70% ethanol and Betadine (Thermo Fisher, 19-027132) followed by a medial incision of the skin to expose the skull. The lateral ventricles were targeted bilaterally using the coordinates: ±1.0 (lateral), –0.44 (posterior), –2.2 (ventral) relative to bregma. Mice were injected with approximately 10⁷ total IU

of lentivirus measured by qPCR Lentivirus Titer kit (abm, LV900) and delivered by two 10 μ l injections using a 25 μ l Hamilton syringe (Sigma-Aldrich, 20787) on a stereotaxic alignment system (Kopf, 1900) and the incision was sutured. Mice received 1 mg kg⁻¹ Buprenorphine-SR via subcutaneous injection and were permitted to recover 7 days in a separate clean cage before induction of EAE.

EAE induction

EAE was induced with 100 μ g of MOG₃₅₋₅₅ (Genemed Synthesis, 110582) emulsified in freshly prepared complete Freund's adjuvant (Incomplete Freund's Adjuvant (BD Biosciences, BD263910) mixed with *Mycobacterium tuberculosis* H-37Ra (BD Biosciences, 231141); final concentration 5 mg ml⁻¹). All animals received 2 subcutaneous injections of 100 μ l each of MOG and a single intraperitoneal injection of 400 ng pertussis toxin (List Biological Laboratories, 180) in 200 μ l of PBS. Mice received a second injection of PTx 48 h after the initial injection. Mice were monitored and clinical scores were documented daily until the end of the experiment. Mice were euthanized at different time points of disease. EAE clinical scores were defined as follows: 0, no signs; 1, fully limp tail; 2, hindlimb weakness; 3, hindlimb paralysis; 4, forelimb paralysis; 5, moribund.

Isolation of cells from the adult CNS

Astrocytes were isolated by flow cytometry as described^{2-4,6-8} and by modifying a previously described protocol⁷⁰. In brief, mice were perfused with 1 \times PBS and the CNS was isolated into 10 ml of enzyme digestion solution consisting of 75 μ l Papain suspension (Worthington, LS003126) diluted in enzyme stock solution (ESS) and equilibrated to 37 C. ESS consisted of 10 ml 10 \times EBSS (Sigma-Aldrich, E7510), 2.4 ml 30% d(+)-Glucose (Sigma-Aldrich, G8769), 5.2 ml 1 M NaHCO₃ (VWR, AAJ62495-AP), 200 μ l 500 mM EDTA (Thermo Fisher Scientific, 15575020), and 168.2 ml ddH₂O, filter-sterilized through a 0.22- μ m filter. Samples were shaken at 80 rpm for 30–40 min at 37 °C. Enzymatic digestion was stopped with 1 ml of 10 \times hi ovomucoid inhibitor solution and 20 μ l 0.4% DNase (Worthington, LS002007) diluted in 10 ml inhibitor stock solution (ISS). Hi ovomucoid inhibitor stock solution (10 \times) contained 300 mg BSA (Sigma-Aldrich, A8806), 300 mg ovomucoid trypsin inhibitor (Worthington, LS003086) diluted in 10 ml 1 \times PBS and filter-sterilized using at 0.22- μ m filter. ISS contained 50 ml 10 \times EBSS (Sigma-Aldrich, E7510), 6 ml 30% d(+)-Glucose (Sigma-Aldrich, G8769), 13 ml 1 M NaHCO₃ (VWR, AAJ62495-AP) diluted in 170.4 ml ddH₂O and filter-sterilized through a 0.22- μ m filter. Tissue was mechanically dissociated using a 5 ml serological pipette and filtered through at 70- μ m cell strainer (Fisher Scientific, 22363548) into a fresh 50 ml conical. Tissue was centrifuged at 500g for 5 min and resuspended in 10 ml of 30% Percoll solution (9 ml Percoll (GE Healthcare Biosciences, 17-5445-01), 3 ml 10 \times PBS, 18 ml ddH₂O). Percoll suspension was centrifuged at 500g for 25 min with no brakes. Supernatant was discarded and the cell pellet was washed 1 \times with 1 \times PBS, centrifuged at 500g for 5 min and prepared for downstream applications.

Isolation of mouse splenic cells

Spleens were isolated prior to mouse perfusion and mechanically dissociated. Red blood cells were lysed with ACK lysing buffer (Life Technology, A10492-01) for 2 min and

washed with 0.5% BSA, 2 mM EDTA pH 8.0 in 1× PBS and prepared for downstream applications.

FACS

Cells were stained in the dark on ice for 20 min with FACS antibodies. Cells were then washed once with 1× PBS and resuspended in 1× PBS for sorting as described^{2-4,6-8}. Antibodies used in this study were: PE anti-mouse CD45R/B220 (BD Biosciences, 553089, 1:100), PE anti-mouse TER-119 (Biolegend, 116207, 1:100), PE anti-O4 (R&D Systems, FAB1326P, 1:100), PE anti-CD105 (eBioscience, 12-1051-82, 1:100), PE anti-CD140a (eBioscience, 12-1401-81, 1:100), PE anti-Ly-6G (Biolegend, 127608, 1:100), BV786-Ly6C (BD Biosciences, 740850, 1:100), APC anti-CD45 (eBioscience, 17-0451-83, 1:100), APC-Cy7 anti-CD11c (BD Biosciences, 561241, 1:100), and FITC anti-CD11b (eBioscience, 11-0112-85, 1:100). All cells were gated on the following parameters: CD105⁻CD140a⁻O4⁻Ter119⁻Ly-6G⁻CD45R⁻. Astrocytes were gated on: CD11b⁻CD45⁻Ly-6C⁻CD11c⁻. Microglia were subsequently gated on: CD11b^{hi}CD45^{low}Ly-6C^{low}. Pro-inflammatory monocytes were gated on: CD11b^{hi}CD45^{hi}Ly-6C^{hi}. Compensation was performed on single-stained samples of cells and an unstained control. Cells were sorted on a FACS Aria IIu (BD Biosciences) and analysed by BD FACSDIVA (v.8.0.1).

FACS analysis of T cells

CNS and splenic cell suspensions were stimulated with 50 ng ml⁻¹ phorbol 12-myristate 13-acetate (PMA, Sigma-Aldrich, P8139), 1 μM Ionomycin (Sigma-Aldrich, I3909-1ML), GolgiStop (BD Biosciences, 554724, 1:1500) and GolgiPlug (BD Biosciences, 555029, 1:1500) diluted in T cell culture medium (RPMI (Life Technologies, 11875119) containing 10% FBS, 1% penicillin/streptomycin, 50 μM 2-metcaptoethanol (Sigma-Aldrich, M6250), and 1% non-essential amino acids (Life Technologies, 11140050)). After 4 h, cell suspensions were washed with 0.5% BSA, 2 mM EDTA in 1× PBS and incubated with surface antibodies and a live/dead cell marker on ice. After 30 min, cells were washed with 0.5% BSA, 2 mM EDTA in 1× PBS and fixed according to the manufacturer's protocol of an intracellular labelling kit (eBiosciences, 00-5523-00). Surface antibodies used in this study were: BUV661 anti-mouse CD45 (BD Biosciences, 565079, 1:100), BV750 anti-mouse CD3 (Biolegend, 100249, 1:50), PE-Cy7 anti-mouse CD4 (eBioscience, 25-0041-82, 1:100), BV785 anti-mouse CD11b (BD Biosciences, 101243, 1:100), BV570 anti-mouse Ly6C (Biolegend, 128030, 1:100), BUV805 anti-mouse CD8a (BD Bioscience, 564920, 1:100), BUV563 anti-mouse Ly6G (BD Biosciences, 565707, 1:100), BUV737 anti-mouse CD11c (BD Biosciences, 612797, 1:100), Pe/Cy5 anti-mouse CD44 (BioLegend, 103010, 1:100), Intracellular antibodies were: APC anti-mouse IFNγ (BD Biosciences, 554413, 1:100), PE anti-mouse IL-17A (eBiosciences, 12-7177-81, 1:100), BV421 anti-mouse GM-CSF (BD Biosciences, 564747, 1:100), FITC anti-mouse FoxP3 (eBiosciences, 11-5773-82, 1:100). Gating of CNS and splenic cells was performed on >10,000 live CD4⁺ cells. FACS was performed on a Symphony A5 (BD Biosciences) and analysed by Flowjo.

Isolation, culture and stimulation of human primary astrocytes

Primary human fetal astrocytes were isolated as previously described^{71–73}. Second trimester fetal brain tissues were obtained from Centre Hospitalier Universitaire Sainte-Justine, Montreal, Canada or from the Birth Defects Research Laboratory, University of Washington, Seattle, WA, USA with maternal written consent and under local ethic boards' approval. Isolation of glial cells was carried out through mechanical and chemical digestion. Primary fetal astrocytes were maintained in Dulbecco's Modified Eagle Medium (DMEM)/F12 (Sigma-Aldrich, D8437) with 10% fetal bovine serum (FBS, Wisent Bio Products, 080–150), 1% penicillin/streptomycin (Thermo Fisher, 15140122) and 1% Glutamax (Thermo Fisher, 35050-061) and grown in incubators set to 37 °C with 5% CO₂. For in vitro conditions, human primary astrocytes were seeded at 50,000 cells per well. The cell media was aspirated, cells were washed with 37 °C PBS and the fresh, appropriate media was then added into the wells. The cells were treated for 18–24 h with 10 ng ml⁻¹ IL-1 β (Gibco, PHC0815) and 5 ng ml⁻¹ TNF (Gibco, PHC3016) in basal media. After the first stimulation, cells were washed 2 times with warmed PBS and then cultured in normal culture media for the subsequent 6 days. At day 7, human primary astrocytes were re-treated (2 \times) or treated (1 \times) with 10 ng ml⁻¹ IL-1 β and 5 ng ml⁻¹ TNF or PBS for 2 h. For the control conditions, the media aspiration, media change and PBS washing occurred alongside all treated cells. At the end of these treatments, total RNA was isolated, transcribed and subjected to qPCR. Inhibitor compound treatment was pre-treated at 37 °C for 2 h before the first cytokine treatment, then co-treated with IL-1 β and TNF for 18–24 h. The inhibitor used in these studies is 5 μ M C646 (Selleck Chemicals S7152).

RNA expression analysis of primary astrocytes

Primary astrocytes were lysed in Buffer RLT (Qiagen) and RNA was isolated from cultured astrocytes using the Qiagen RNeasy Mini kit (Qiagen, 74106). cDNA was transcribed using the High-Capacity cDNA Reverse Transcription Kit (Life Technologies, 4368813). Gene expression was then measured by qPCR using Taqman Fast Universal PCR Master Mix (Life Technologies, 4367846). Taqman probes used in this study are: *Actb* (Mm02619580_g1), *Nos2* (Mm00440502_m1), *Ccl2* (Mm00441242_m1), *Il6* (Mm00446190_m1), *Ep300* (Mm00625535_m1), *Kat5* (Mm01231512_m1), *Kat2b* (Mm00517402_m1), *Acly* (Mm01302282_m1), *Acss2* (Mm00480101_m1), *ACTB* (Hs01060665_g1), *NOS2* (Hs01075529_m1), *IL6* (Hs00174131_m1), and *CCL2* (Hs00234140_m1). qPCR data were analysed by the ddC_t method by normalizing the expression of each gene for each replicate to *Actb* and then to the control group.

Chromatin immunoprecipitation

Approximately >1 million astrocytes were used by cell preparation according to the ChIP-IT Express Enzymatic Shearing and ChIP protocol (Active Motif, 53009). In brief, cells were fixed in 1% formaldehyde for 10 min with gentle agitation, washed in 1 \times PBS, washed for 5 min in 1 \times glycine Stop-Fix solution in PBS, and scraped in 1 \times PBS supplemented with 500 μ M PMSF. Cells were pelleted, nuclei isolated, and chromatin sheared using the Enzymatic Shearing Cocktail (Active Motif) for 10 min at 37 °C with vortexing every 2 min. Sheared chromatin was immunoprecipitated according to the Active Motif protocol overnight at 4

°C with rotation. The next day, the protein-bound magnetic beads were washed 1× with ChIP buffer 1, 1× with ChIP buffer 2, and 1× with 1× TE. Cross-links were reversed in 100 µl of 0.1% SDS and 300 mM NaCl in 1×TE at 63 °C for 4–5 h, as described^{4,74}. DNA was purified using Agencourt AMPure XP Beads (Beckman Coulter, A63881). qPCR was performed using Fast SYBR Green Master Mix (Thermo Fisher Scientific, 4385612). Anti-IgG immunoprecipitation and input were used as controls. We used rabbit anti-p300 (Genetex, GTX114541, 1:100), rabbit anti-H3K27ac (Abcam, 1:100, ab4729), and rabbit IgG polyclonal isotype control (Cell Signaling, 2975 S, 1:100). PCR primers were designed with Primer3⁷⁵ to generate 50–150 bp amplicons. Primer sequences used: p300-II6-F: 5'-GCTGTTTCAGCTGCCTTTTT-3', p300-II6-R: 5'-AAAGCCGGTTGATTCTTGTG-3', p300-Ccl2-F: 5'-GG CCCGTTAGCTGTCTGTTA-3', p300-Ccl2-R: 5'-AGTGGTTGGA ACCCTTCACA-3', p300-Nos2-F: 5'-AACACGAGGCTGAGCTGAC T-3', p300-Nos2-R: 5'-CACACATGGCATGGAATTTT-3', p65-II6-F: 5'-AAGCACACTTCCCCTTCCT-3', p65-II6-R: 5'-GCTCCAGAGC AGAATGAGCTA-3', p65-Ccl2-F: 5'-CCAAATCCAACCCACAGTT-3', p65-Ccl2-R: 5'-AGTGAGAGTTGGCTGGTGCT-3'. Data were analysed by ddC_i relative to Input control.

Bulk RNA sequencing

Sorted cells were lysed and RNA isolated using the Qiagen RNeasy Micro kit (Qiagen, 74004) with on-column DNase I digestion (Qiagen, 79254). RNA was suspended in 10 µl of nuclease-free water at 0.5–1 ng µl⁻¹ and sequenced using SMARTSeq2⁷⁶ at the Broad Institute Technology Labs and the Broad Genomics Platform. Processed RNA-seq data was filtered by removing genes with low read counts. Read counts were normalized using trimmed mean of M-values normalization and counts per million were calculated to create a matrix of normalized expression values. The fastq files of each RNA-seq data sample were aligned to the *Mus musculus* GRCm38 transcriptome using Kallisto (v0.46.1), and the same software was used to quantify the alignment results. Differential expression analysis was conducted using DESeq2, and the log₂ fold change was adjusted using apeGLM for downstream analysis.

ChIP-seq

Approximately 500,000 cells were fixed, nuclei collected, and chromatin isolated using the ChIP-IT Express Enzymatic Shearing Kit (Active Motif, 53009). Chromatin complexes were immunoprecipitated using a rabbit anti-Histone H3 (acetyl K27) antibody (Abcam ab4729, 1:100) and rabbit IgG polyclonal isotype control (Cell Signaling, 2975 S, 1:100). Cross-links were reversed in 100 µl of 0.1% SDS and 300 mM NaCl in 1× TE at 63 °C for 4–5 h, as described^{4,74}. DNA was purified using Agencourt AMPure XP Beads (Beckman Coulter, A63881). DNA was analysed using a 2100 Bioanalyzer (Agilent) and High Sensitivity DNA Kit (Agilent Technologies, 5067-4626). DNA libraries were then prepared for sequencing using the NEBNext Ultra II DNA Library Prep Kit (New England Biolabs, E7645S) and sequencing adapters were ligated using NEBNext Multiplex Oligos for Illumina (E7500S, E7335S) as described. ChIPed DNA was amplified by using 14 cycles according to the NEBNext protocol. DNA libraries were not size-selected, but primer dimers were removed via purification using Agencourt AMPure XP Beads (Beckman Coulter, A63881). DNA

libraries consisting of ChIPed DNA and IgG control DNA for each sample were sequenced on an Illumina HiSeq 4,000 using 2×75 paired end sequencing.

Raw fastq files were first checked for quality using Multiqc sequence analysis. Reads were aligned to the mouse genome (mm10) using bowtie2 (2.3.4.3)⁷⁷. Subsequently, SAM files were sorted and filtered using Sambamba (v.0.8.2)⁷⁸. We discarded unmapped and duplicate fragments. Sorted BAM files were indexed using samtools (v.1.15.1)⁷⁹. BAM files were then converted to BigWig files for visualization using deepTools (v.3.5.0)⁸⁰. Normalization for all BigWig files were carried out against effective genome size (2652783500 for mice H3K27ac ChIP-seq). Peak analysis was carried out with MACS2 callpeak (v.2.2.7)⁸¹ using stringent parameters (-f BAMPE --mfold 5 50 -p 0.001). A master-peak bed file was created using bedtools merge function. Significant peaks present in one sample were considered. Aligned and filtered counts were extracted from BAM files using master-peak bed file and differential peaks between p300 and scramble were determined using two-sided t-test with p -value < 0.05 (Supplementary Table 5). Specific peaks were visualized using IGV (v.2.11.4), exported as.png, and edited in Adobe Illustrator. Peak plots were visualized using deepTools computeMatrix with 500 bp from peak centre.

ATAC-seq

Sequencing libraries were prepared largely as described previously^{4,82,83}. After isolation of nuclei, transposition was performed using the kit (Illumina, FC-121-1030). DNA was then amplified using NEBNext High Fidelity $2 \times$ PCR Master Mix (New England Biolabs, M0541S) for 5 cycles. DNA quantity was then measured using a Viiia 7 Real-Time PCR System (Thermo Fisher Scientific) and the number of cycles required to achieve 1/3 of maximal SYBR Green fluorescence was determined and libraries were amplified accordingly. TruSeq adapters (universal: Ad1_noMX and barcoded: Ad2.1-Ad2.24) were used according to the Buenrostro protocol. Libraries were purified using MiniElute PCR Purification Kit (Qiagen, 28006) followed by double-sided Agencourt AMPure XP bead purification (Beckman Coulter, A63881) to remove primer dimers and large DNA fragments. Libraries were analysed on a 2100 Bioanalyzer (Agilent Technologies) and High Sensitivity DNA Kit (Agilent Technologies, 5067-4626). Libraries were sequenced by Genewiz on an Illumina HiSeq 4000 by 2×75 bp paired end sequencing.

Paired end ATAC-seq reads were first assessed using FASTQC. Reads were trimmed using cutadapt to remove adapters and low quality reads below 30. Pair-end reads were then aligned against the GRCm39/mm10 mouse genome assembly with Bowtie (v2.3.0)⁸⁴ in local mode, sensitive settings, and a maximum fragment size of 2,000. Duplicated reads were marked using Picard (v.2.5.0). Alignments were filtered with SAM-tools (v1.3) to exclude reads with mapping quality < 30 , not properly paired, duplicated, aligned to mitochondrial genome, and/or aligned to ENCODE blacklist regions. Alignments with an insertion size of > 100 bp were removed to enrich for nucleosome-free reads. ATAC-seq peaks were called for each replicate using MACS2, using --format BAMPE and --keep-dup all. IDR (v2.0.2) was used to determine consistency of peak detection between individual replicates and peaks with a threshold below 0.10 were merged between replicates for downstream analysis. For differential peaks, merged peaks were mapped to specific genic

regions using bedtools intersect and reads were counted using subread featureCounts (v.1.6.2) to produce a count matrix. DESeq2 was then used to find differential peaks.

FIND-seq

The transcriptome of *Acly⁺Ep300⁺* astrocyte subsets was isolated and sequenced using the FIND-seq/Smart-seq3 protocol^{29,84}. The process started with the preparation of oligo dT primer-conjugated agarose. 50 μM of acrydite-modified primers (/5Acryd/TTTTTTACGAGCATCAGCAGCATACGAT30V, IDT) were mixed with a 0.5% (wt/vol) allyl agarose solution (SFR allyl agarose, Lucidant Polymers), and 0.1% (wt/vol) APS (Promega, V3131) and 0.1% (vol/vol) TEMED (Invitrogen, 15524-010) were introduced at the reaction initiation and after a 4 h incubation at 45 °C to conjugate Oligo dT primer on the agarose chain. For optimal conjugation, the reaction was continued for an additional 16 h. Extra ultra-low gelling temperature agarose type IX-A (Sigma-Aldrich, A2576) was used to raise total agarose concentration to 2%. The conjugated agarose gel was washed in nuclease-free water to remove unreacted primers and residual chemicals. The concentration of the oligo dT primer on the agarose was quantified using the Qubit ssDNA assay kit (Invitrogen, Q10212) and normalized to 8 μM .

Astrocytes were resuspended at a density of $6.11 \times 10^6 \text{ ml}^{-1}$ in a buffer composed of 1% (vol/vol) Pluronic F-68 (Thermo Fisher, 24040032) and 18% (vol/vol) Opti-prep (Sigma-Aldrich, D1556-250ML) in HBSS buffer without calcium or magnesium (Gibco, 14170112), then filtered through a 70- μm cell strainer (Fisher Scientific, 22363548) and loaded into a 1 ml syringe (BD Biosciences, 309628). A lysis buffer, containing 20 mM Tris-HCl (pH 7.5) (Teknova, T5075), 1,000 mM LiCl (Sigma-Aldrich, L7026), 1% (wt/vol) LiDS (Sigma-Aldrich, L4632-25G), 10 mM EDTA (VWR, E177), 10 mM DTT (Sigma-Aldrich, 43816), and 2 $\mu\text{g } \mu\text{l}^{-1}$ Proteinase K (New England Biolabs, P8107S), was prepared and loaded into a 3 ml syringe (BD Biosciences, 309657). Primer-conjugated agarose was completely melted at 95 °C for over 2 h and subsequently loaded into a 3 ml syringe, which was placed into a custom-built syringe heater to maintain its molten state at 90 °C. Single cells, alongside the primer-conjugated agarose and lysis buffer, were encapsulated using a bubble-triggered device (Extended Data Fig. 8b). The cell solution, lysis buffer, molten agarose solution, Droplet Generation Oil for Probes (Bio-Rad, 1864110), and pressurized air lines were connected to the Bubble-triggered device via PE/2 tubing (Scientific Commodities, BB31695-PE/2). The flow rates were adjusted to produce 55- μm droplets: cell: 600 $\mu\text{l h}^{-1}$, lysis buffer: 600 $\mu\text{l/hr}$, molten primer-conjugated agarose: 1,200 $\mu\text{l h}^{-1}$, Droplet Generation Oil for Probes: 5,000 $\mu\text{l h}^{-1}$, Pressured air: 20 psi. Following encapsulation, the droplets were incubated at 55 °C for 2 h and subsequently cooled at 4 °C for 1 h to solidify the agarose within the droplets. The hardened agarose beads were collected through a droplet-breaking procedure. Residual oil at the bottom of the tube was discarded, and the emulsion was effectively disrupted using 20% (vol/vol) 1H,1H,2H,2H-Perfluoro-1-octanol (PFO) (Sigma-Aldrich, 370533-25 G) in HFE-7500 (3 MTM NovecTM 7500 Engineered Fluid). The mixture was centrifuged for 5 min at 2,000 g at 4 °C, and the OFP phase at the bottom was removed. The agarose beads were then resuspended in a buffer containing 20 mM Tris-HCl (pH 7.5), 500 mM LiCl, 0.1% (wt/vol) LiDS, and 0.1 mM EDTA. Following another centrifugation for 5 min at 2,000 g at 4 °C, the supernatant was discarded. The beads

were subsequently resuspended in a buffer composed of 20 mM Tris-HCl (pH 7.5) and 500 mM NaCl (Thermo Fisher Scientific, AM9759).

Released mRNA from the cells was captured through hybridization with the conjugated oligo dT primer. Subsequent reverse transcription leads to the formation of cDNA on the agarose bead. For the reverse transcription reaction, agarose beads were combined with a master mix comprising 1 mM dNTPs (Thermo Scientific, R1121), 2 μ M Smart-seq3 TSO (AAGCAGTGGTATCAACGCAGAGTACATrGrGrG, IDT), 6 mM MgCl₂ (Sigma-Aldrich, M1028), 1 M betaine (Sigma-Aldrich, 61962), 7.5% PEG-8000 (Promega, V3011), 2 U μ l⁻¹ Maxima H-minus reverse transcriptase, and 0.5 U/ μ l RNase inhibitor (Lucigen, 30281). The reverse transcription reaction was executed by rotating for 30 min at room temperature, followed by further incubation for 1 h 30 min at 42 °C. After reverse transcription, the agarose beads were washed five times in a centrifuge with a solution of 0.1% Tween-20 (Sigma-Aldrich, P9416).

The cDNA on the agarose bead was validated via whole transcriptome amplification (WTA). The genomic material trapped in the agarose bead was stained with SYBR green I (Sigma, S9430), and the concentration of genome-captured beads was measured using a haemocytometer, which counted the SYBR green I-stained agarose beads (Extended Data Fig. 8e). Based on the calculated concentration, 750 genome-capture beads were resuspended in 25 μ l of WTA master mix; this contained 1 \times KAPA HiFi master mix (Roche, KK2601), 0.5 μ M Smart-seq3 forward primer (TCGTCGGCAGCGTCAGATGTGTATAAGA GACAGATTGCGCAATG, IDT), and 0.1 μ M Smart-seq3 reverse primer (ACGAGCATCAGCAGCATACG, IDT). The reaction underwent thermocycling: 95 °C for 3 min, followed by 18 cycles of (98 °C for 15 s, 67 °C for 20 s, 68 °C for 4 min), then 72 °C for 5 min, and held at 4 °C. The WTA product was extracted using 0.8 \times volume of AMPure XP beads (Beckman Coulter, A63881) following the manufacturer's protocol. DNA was measured with the Qubit dsDNA HS Assay kit. The size distribution of 1 ng of WTA product, based on the Qubit results, was confirmed on a Bioanalyzer (Extended Data Fig. 8f).

The genome and transcriptome-capturing agarose beads were reintroduced into droplets to execute multiplexed droplet digital PCR (ddPCR). The PCR master mix (TaqPath ProAmp Master Mix; Thermo Fisher Scientific, A30866) was combined with taqman probes for *Ep300* (Mm00625535_m1) and *Acly* (Mm01302282_m1), alongside 0.1% Tween-20 and 2.5% PEG 8,000 to ensure droplet stability. This bead reinjection was made by a microfluidic device, the Re-injector device (Extended Data Fig. 8c). The agarose beads were soaked in the PCR master mix for 30 min at room temperature, centrifuged for 3 min at 2,000g at 4 °C, and the supernatant was discarded. The bead pellet was loaded into a 1 ml syringe. A PCR master mix without beads was loaded into a 1 ml syringe, and Droplet Generation Oil for EvaGreen (Bio-Rad, 1864112) was loaded into a 10 ml syringe. The bead, PCR master mix, and oil were connected to the Re-injector device via PE/2 tubing. The flow rates were optimized to generate a single bead per 80- μ m sized droplet with PCR master mix; Bead: 200 μ l h⁻¹, PCR master mix: 300 μ l/hr, Oil: 1800 μ l/hr. Droplets containing the reinjected bead were collected in a PCR tube and underwent thermocycling to generate TaqMan signals. The thermocycling conditions were set as follows: 88 °C for

10 min, followed by 55 cycles of (88 °C for 30 s, 59 °C for 1 min), then 72 °C, and held at 59 °C. After thermocycling, the emulsion was loaded into a 3 ml syringe. The detection and sorting of droplets were performed using an in-house droplet sorting system⁸⁴, and a droplet sorter device (Extended Data Fig. 8d). Two 30 ml syringes filled with HFE-7500 oil and a 3 ml syringe with Droplet Generation Oil for EvaGreen were prepared. A 2 M NaCl solution filled the electrode and moat channels using a 10 ml syringe, and a high voltage amplifier was connected to the needle of the syringe linked to the electrode channel. The droplet sorter device was connected to the emulsion, drop spacing oil (Droplet Generation Oil for EvaGreen in 3 ml syringe), additional spacer oil (HFE-7500 in 30 ml syringe), bias oil (HFE-7500 in syringe) and pressurized air via PE/2 tubing. The assigned flow rates were as follows: Emulsion: 100 $\mu\text{l h}^{-1}$, Droplet spacing oil: 300 $\mu\text{l h}^{-1}$, additional spacing oil: 3,000 $\mu\text{l h}^{-1}$, bias oil: 4,000 $\mu\text{l h}^{-1}$, pressured air: 20 psi. The TaqMan signals were excited using two lasers (OptoEngine, MLL-FN-473, MLL-III-532), and detected with bandpass filters (GFP channel FF552 and FF01-517/20; RFP channel FF593 and FF01-572/28) and photomultiplier tubes (PMTs) (Thorlabs, PMM01, PMM02) setup. Negative, singles, and double positive droplets were sorted directly into a 1.5 ml tube in aliquot of 100 drops, and 50 μl of nuclease-free water was added on the oil phase.

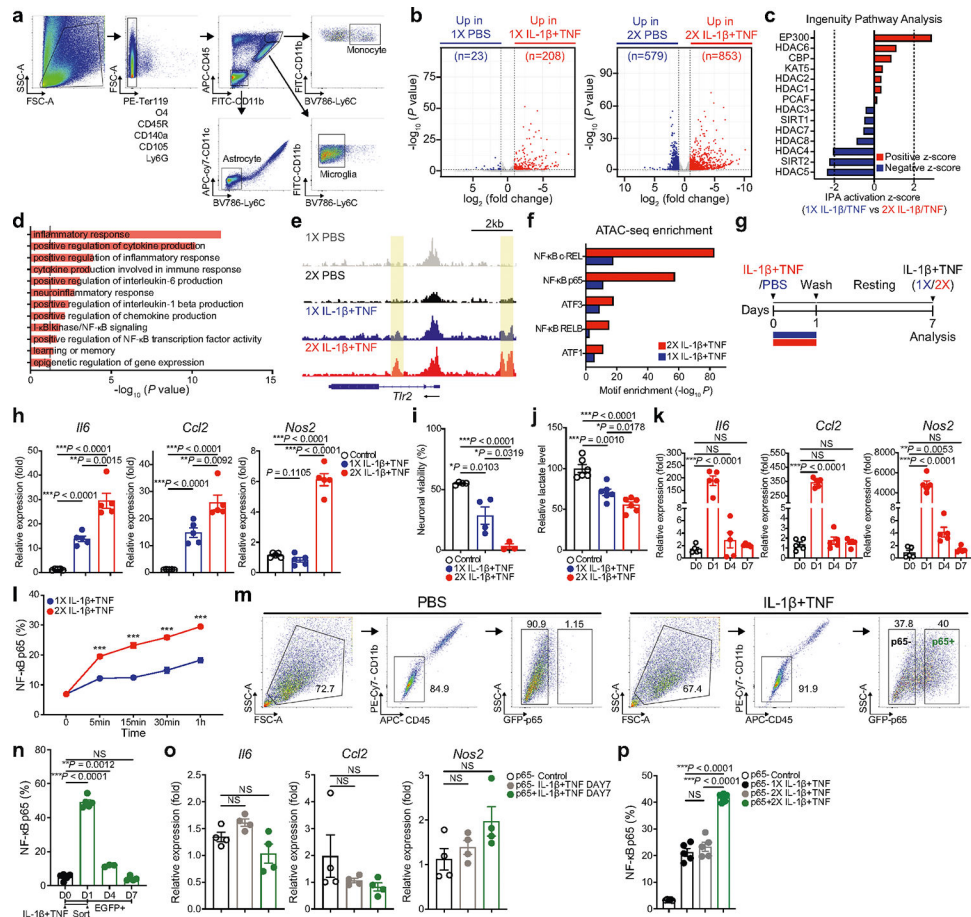
The 1.5 ml tube containing sorted droplets was incubated at $-80\text{ }^{\circ}\text{C}$ for 2 h, then thawed at $60\text{ }^{\circ}\text{C}$ for 10 min to facilitate droplet breaking and release of the cDNA conjugated to the agarose. The oil phase at the bottom was discarded, and the cDNA-containing water phase was collected and transferred to a PCR tube. For the amplification of cDNA, a PCR master mix was added to the PCR tube. This mix contained 0.3 mM dNTP, $1\times$ KAFA HiFi enzyme and buffer (Roche, KK2502), 0.5 μM Smart-seq3 forward primer and 0.1 μM Smart-seq3 reverse primer. The reaction was subjected to the following thermocycling conditions: $95\text{ }^{\circ}\text{C}$ for 3 min, followed by 24 cycles of ($98\text{ }^{\circ}\text{C}$ for 15 s, $67\text{ }^{\circ}\text{C}$ for 20 s, $68\text{ }^{\circ}\text{C}$ for 4 min), then $72\text{ }^{\circ}\text{C}$ for 5 min, and held at $4\text{ }^{\circ}\text{C}$. The amplified material was cleaned up with $0.8\times$ volume of AMPure XP beads and eluted in 10 μl of nuclease-free water. Finally, the DNA library was prepared using the Nextera XT Library Prep Kit (Illumina, FC-131-1024), following the manufacturer's protocol.

Pathway analysis

GSEA or GSEAPreranked analyses were used to generate enrichment plots for bulk RNA-seq or scRNA-seq data^{85,86} using MSigDB molecular signatures for canonical pathways: KEGG/Reactome/Biocarta (c2.cp.all), Motif (c3.all), Gene ontology (c5.cp.all), and Hallmark (h.all). To determine regulators of gene expression networks, IPA software (Qiagen) was used by inputting gene expression datasets with corresponding log (FoldChange) expression levels compared to other groups. 'Canonical pathways' and 'upstream analysis' metrics were considered significant at $P < 0.05$. Gene sets used for signature scores are indicated in the corresponding figure. The RNA-Seq samples were processed using the following pipeline: FASTQC was used to assess the read quality, and then Kallisto was used to do the pseudo-alignment and quantification. DESeq2 was used to find the differentially expressed genes. From the differential expression analysis, the \log_2 -transformed fold change of the genes were multiplied by the $-\log_{10}$ (adjusted P value), and the products were ordered in a decreasing order, which formed an elbow plot and

knee plot. Genes that are before the elbow point and after the knee points formed the astrocyte epigenetic memory signatures (up and down). Independent component analysis was used to analyse the FIND-Seq dataset to extract the combined signatures. Previously published datasets were analysed from the following studies at their respective accession numbers^{2,30,31}. Seurat (v3) was used to analyse the scRNA-seq dataset. The function AddModuleScore() is used to quantify the scores of signatures derived from bulk RNA-Seq analyses for every cell. Monocle (v2) was then used to construct the pseudotime trajectory for the scRNA-seq dataset.

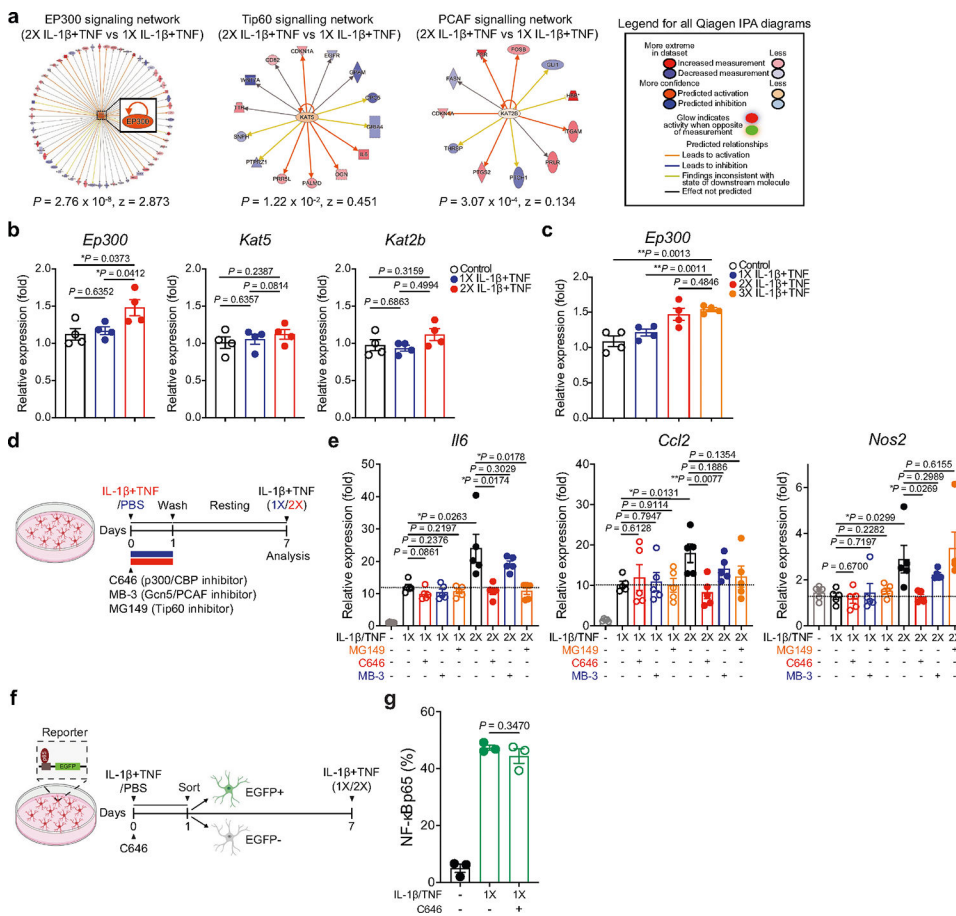
Extended Data



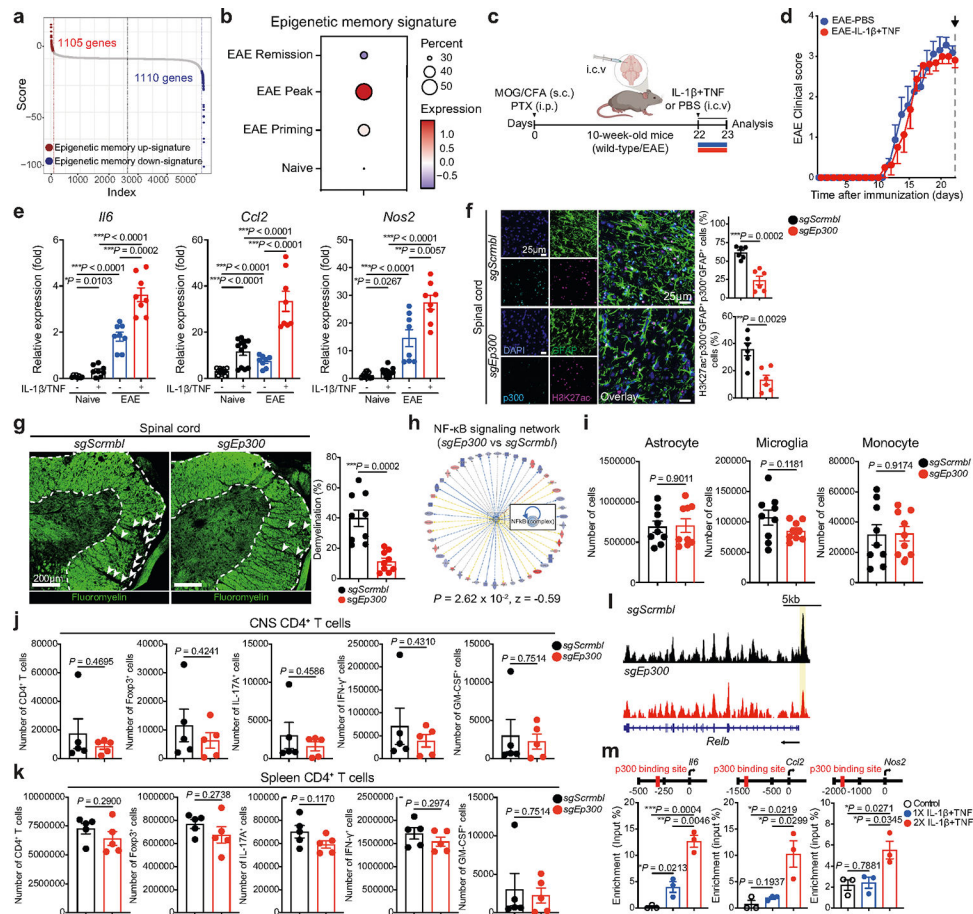
Extended Data Fig. 1 | Analysis of astrocyte epigenetic memory in vivo and in vitro.

(a) Fluorescence-activated cell sorting (FACS) sorting schematic for astrocytes, microglia, and monocytes. **(b)** Volcano plot of differential gene expression increased (red) or decreased (blue) analyzed by RNA-seq of sorted astrocytes. **(c)** IPA predicted upstream regulators in isolated astrocytes. Up-regulated (red) or down-regulated (blue) in astrocytes stimulated twice (2X IL-1β + TNF) versus once (1X IL-1β + TNF) are shown. **(d)** GO pathway analysis of ATAC-seq accessible peaks of isolated astrocytes comparing 2X IL-1β + TNF versus 1X IL-1β + TNF. **(e)** Genome browser snapshots showing the ATAC-seq sequencing tracks at the *Tlr2* locus. Only regions showing a significant increase (p -value < 0.05) in

accessibility in astrocytes from mice stimulated twice (2X) versus once (1X) are highlighted by yellow boxes. **(f)** Homer DNA-motif enrichment analyses of differentially accessible peaks. **(g)** Experimental design for (h) to (j). Primary astrocytes received IL-1 β /TNF stimulation once (1X) or twice (2X). **(h)** qPCR of astrocytes after 30 min activation with IL-1 β /TNF on day 7 (n = 5 per group). Unpaired two-sided *t*-test. **(i)** Neuronal viability assay (n = 4 control; n = 4 1X; n = 3 2X). Unpaired two-sided *t*-test. **(j)** Effect of IL-1 β /TNF stimulation on lactate release (n = 6 per group). Unpaired two-sided *t*-test. **(k)** qPCR analysis of astrocyte response after the first IL-1 β /TNF stimulation (n = 5 per group). Unpaired two-sided *t*-test. **(l)** FACS analysis of EGFP expression in IL-1 β /TNF stimulated primary astrocytes isolated from *p65^{EGFP}* reporter mice (0 min; n = 5; Other time point; n = 6 per group). ****P* < 0.0001. Unpaired two-sided *t*-test. **(m)** FACS sorting schematic of EGFP positive/negative astrocytes after PBS or IL-1 β /TNF stimulation for 18–24 h. **(n)** Primary astrocytes isolated from *p65^{EGFP}* reporter mice received IL-1 β /TNF stimulation. After 18–24 h, EGFP positive astrocytes were sorted and analyzed by FACS of EGFP expression (n = 3–5 per group). Unpaired two-sided *t*-test. **(o)** Primary astrocytes isolated from *p65^{EGFP}* reporter mice received PBS or IL-1 β /TNF stimulation. After 18–24 h, EGFP positive/negative astrocytes were sorted and cultured for 6 days to perform qPCR (n = 4 per group). Unpaired two-sided *t*-test. **(p)** p65 activation in EGFP positive/negative astrocytes 1 h after IL-1 β /TNF stimulation on day 7 (n = 5 per group). Unpaired two-sided *t*-test. Data shown as mean \pm s.e.m.



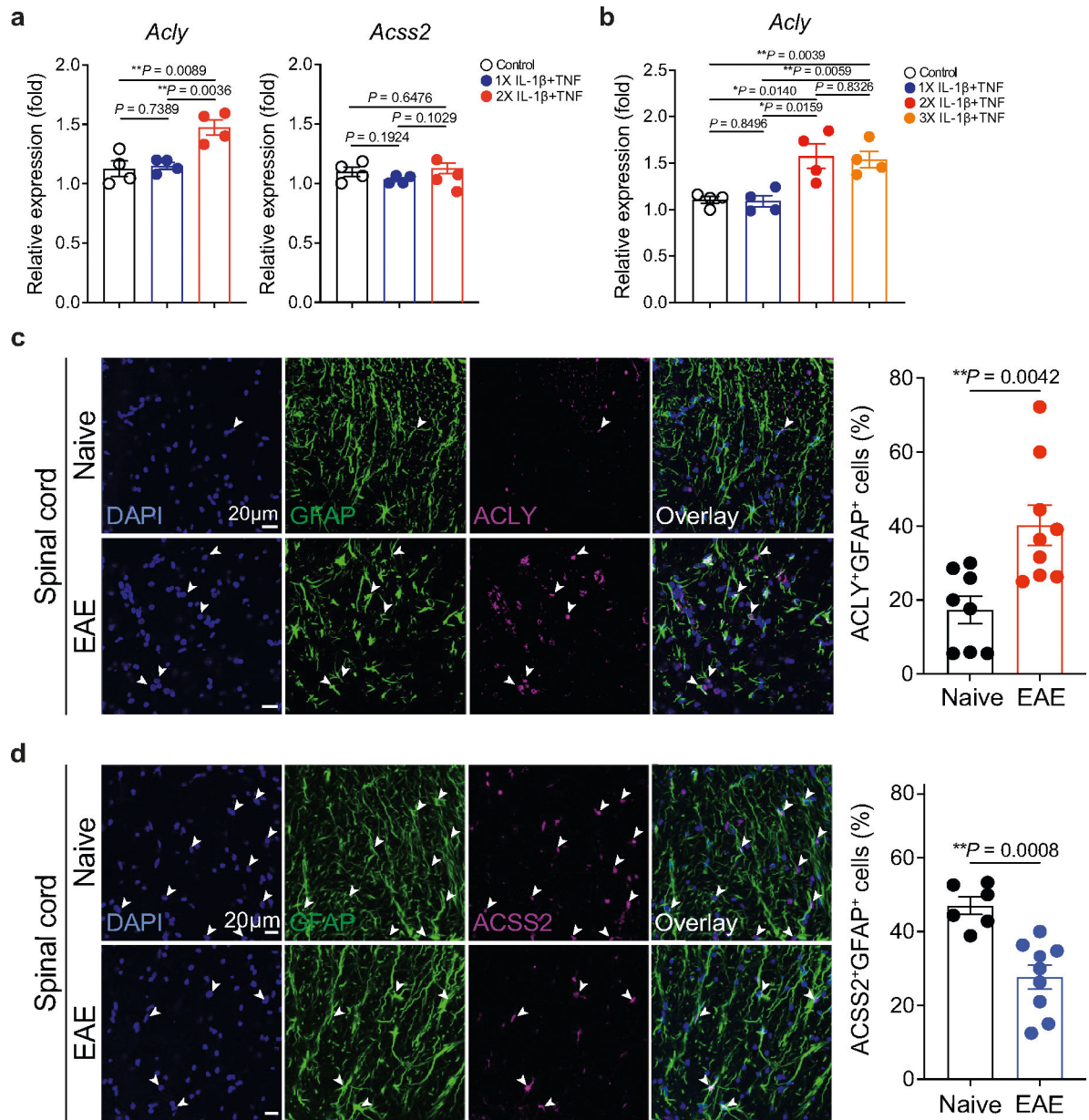
Extended Data Fig. 2 | HAT enzyme expression and regulation of astrocyte epigenetic memory. (a) EP300, Tip60 (KAT5), and PCAF (KAT2B) signaling network in isolated brain astrocytes that received ICV administration of IL-1 β /TNF twice (2X) compared to once (1X). (b) qPCR analysis of *Ep300*, *Kat5*, and *Kat2b* expression in primary astrocytes stimulated after 30 min IL-1 β /TNF stimulation on day 7 (n = 4 per group). Unpaired two-sided *t*-test. (c) Primary astrocytes were stimulated with IL-1 β /TNF once (1X), twice (2X), or three times (3X). qPCR analysis of astrocytes after 30 min activation with IL-1 β /TNF on day 14 (n = 4 per group). Unpaired two-sided *t*-test. (d) Experimental design for (e). (e) qPCR of primary astrocytes in the presence with/without C646 (p300/CBP inhibitor), MB-3 (Gcn5/PCAF inhibitor), and MG149 (Tip60 inhibitor) after 30 min stimulation with IL-1 β /TNF on day 7 (n = 5 per group). Unpaired two-sided *t*-test. (f) Experimental design for Fig. 1j. (g) Gene expression 30 min after IL-1 β /TNF stimulation on day 7 of EGFP positive/negative astrocytes treated with C646 or vehicle (n = 8 per group). Unpaired two-sided *t*-test. Data shown as mean \pm s.e.m.



Extended Data Fig. 3 | Astrocyte epigenetic memory and *Ep300* signaling in EAE.

(a) Generation of astrocyte epigenetic memory signature filtered based on adjusted p -value and fold change. Up-signature (red) or down-signature (blue) in astrocytes stimulated twice (2X) than once (1X) are shown. (b) Astrocyte epigenetic memory signature score applied to naive and EAE scRNA-seq astrocyte dataset (Priming, Peak, and Remission)¹⁰. (c) Experimental design for (d,e). (d) EAE score for (e) ($n = 8$ per group). Data shown as mean \pm s.e.m. Naive and EAE induced C57BL/6 mice received ICV administration of IL-1 β /TNF (EAE peak, Day 22), and 18–24 h later sorted brain astrocytes were analyzed. (e) qPCR of IL-1 β /TNF response of astrocytes (Naive; $n = 12$; EAE; $n = 8$ per group). Representative data of two independent experiments. Unpaired two-sided t -test. (f) Immunostaining (left) and quantification (right) of H3K27ac⁺ and p300⁺ astrocytes from *sgScrmbl*- and *sgEp300*-transduced mice at 23 days after EAE induction ($n = 6$ spinal cord sections; $n = 3$ mice per group). Unpaired two-sided t -test. (g) FluoroMyelin dye staining and percentage of myelin loss in spinal cord from *sgScrmbl*- and *sgEp300*-transduced mice ($n = 9$ spinal cord sections; $n = 3$ mice per group). Lesions indicated by arrowheads. Unpaired two-sided t -test. (h) NF- κ B signaling network comparing *sgEp300*-transduced versus *sgScrmbl*-transduced astrocytes. (i) Quantification of CNS-resident cells from *sgScrmbl*- and *sgEp300*-transduced mice ($n = 9$ per group). Unpaired two-sided t -test. (j,k) Analysis of CNS T cells (up) and splenic T cells (bottom) from *sgScrmbl*- or *sgEp300*-transduced mice ($n = 5$ per group). Unpaired two-sided t -test. (l) Genome browser snapshots showing the *Relb* locus. Only regions

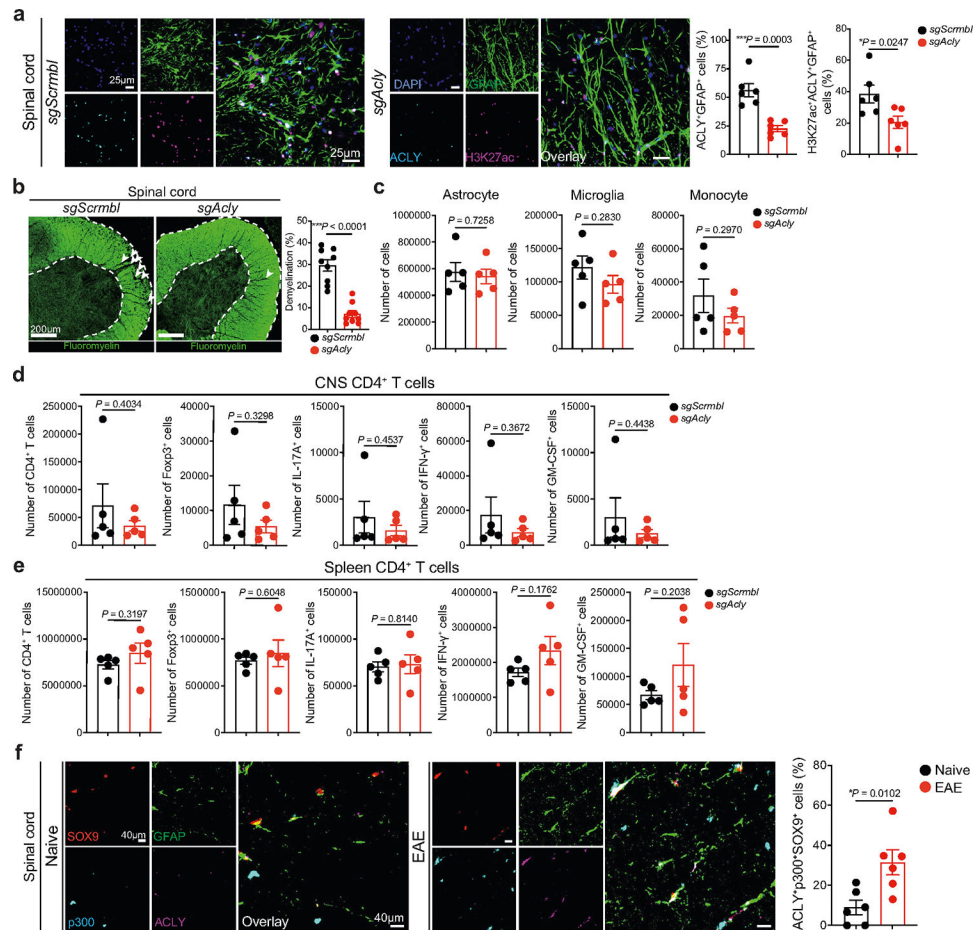
showing a significant decrease (p -value < 0.05) in accessibility in *sgScrambl*-transduced versus *sgEp300*-transduced astrocytes are highlighted by yellow boxes. **(m)** Chip-qPCR analysis of p300 recruitment to promoters in primary astrocytes 30 min after IL-1 β /TNF stimulation on day 7 ($n = 3$ per group). Unpaired two-sided t -test. Data shown as mean \pm s.e.m.



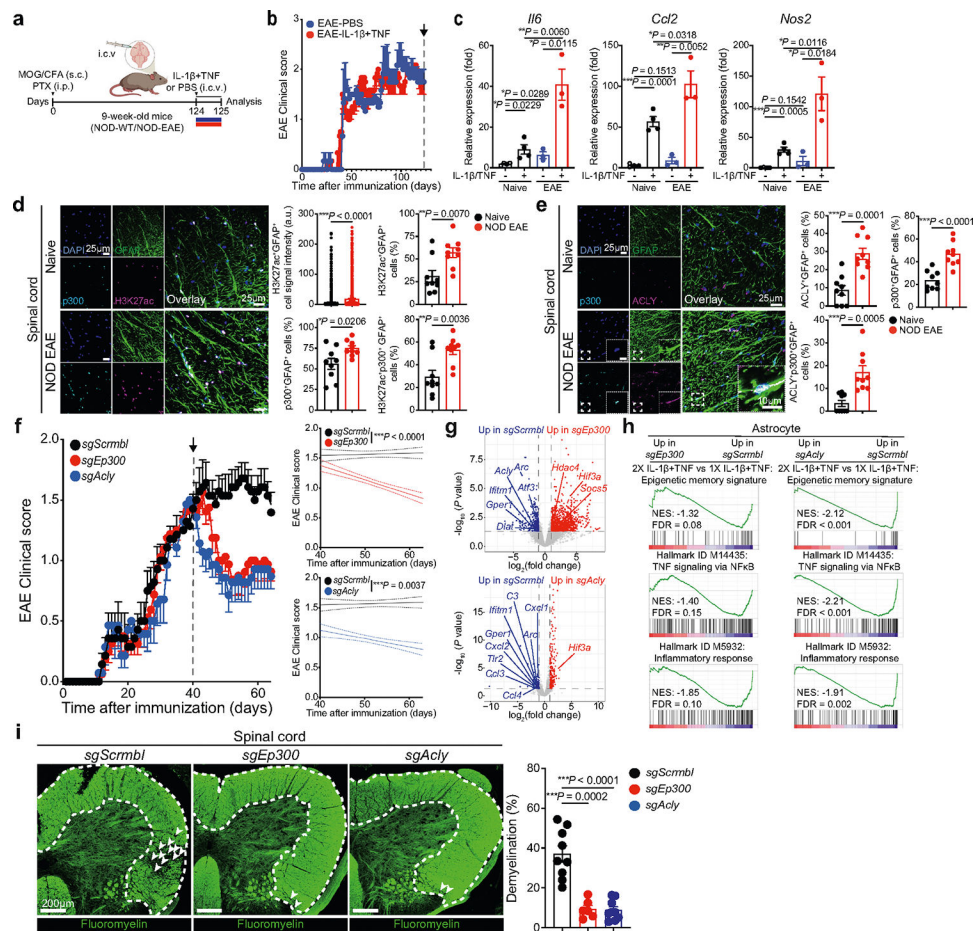
Extended Data Fig. 4 | ACLY and ACSS2 signaling in EAE astrocytes.

(a) qPCR analysis of *Acly* and *Acss2* expression in primary astrocytes stimulated for 30 min with IL-1 β /TNF on day 7 ($n = 4$ per group). Unpaired two-sided t -test. **(b)** Primary astrocytes received IL-1 β /TNF stimulation once (1X), twice (2X), or three times (3X). qPCR analysis of astrocytes after 30 min activation with IL-1 β /TNF on day 14 ($n = 4$ per group). Unpaired two-sided t -test. **(c)** Immunostaining (left) and quantification (right) of ACLY⁺

astrocytes in mice with/without EAE (n = 8 spinal cord sections (naïve); n = 9 spinal cord sections (EAE); n = 3 mice per group). Unpaired two-sided *t*-test. **(d)** Immunostaining (left) and quantification (right) of ACS2⁺ astrocytes in mice with/without EAE (n = 6 spinal cord sections (naïve); n = 9 spinal cord sections (EAE); n = 3 mice per group). Unpaired two-sided *t*-test. Data shown as mean ± s.e.m.



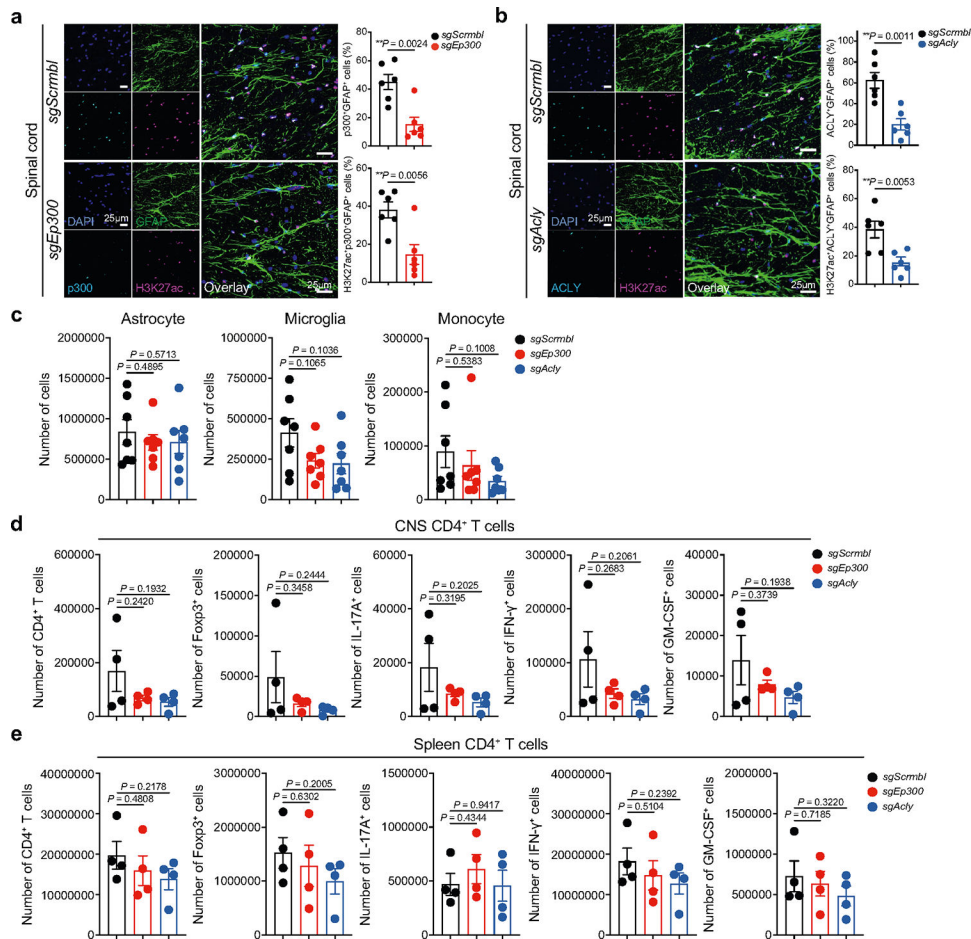
Extended Data Fig. 5 | Astrocyte *Acly* signaling and ACLY + p300⁺ astrocytes in EAE. **(a)** Immunostaining (left) and quantification (right) of H3K27ac⁺ and ACLY⁺ astrocytes from *sgScrmbl*⁻ and *sgAcly*⁻ transduced mice at 21 days after EAE induction (n = 6 spinal cord sections; n = 3 mice per group). Unpaired two-sided *t*-test. **(b)** Staining with FluoroMyelin dye and percentage of myelin loss in spinal cord of *sgScrmbl*⁻ and *sgAcly*⁻ treated mice (n = 9 spinal cord sections; n = 3 mice per group). Lesions indicated by arrowheads. Unpaired two-sided *t*-test. **(c)** Quantification of CNS-resident cells from *sgScrmbl*⁻ and *sgAcly*⁻ transduced mice (n = 5 per group). Unpaired two-sided *t*-test. **(d,e)** Analysis of CNS T cells (up) and splenic T cells (bottom) from *sgScrmbl*⁻ or *sgAcly*⁻ transduced mice (n = 5 per group). Unpaired two-sided *t*-test. Data shown as mean ± s.e.m. **(f)** Immunostaining (left) and quantification (right) of ACLY⁺SOX9⁺, p300⁺SOX9⁺, and ACLY⁺p300⁺SOX9⁺ astrocytes in EAE and control mice (n = 6 spinal cord sections; n = 3 mice per group). Unpaired two-sided *t*-test. Data shown as mean ± s.e.m.



Extended Data Fig. 6 | Astrocyte epigenetic memory in NOD EAE.

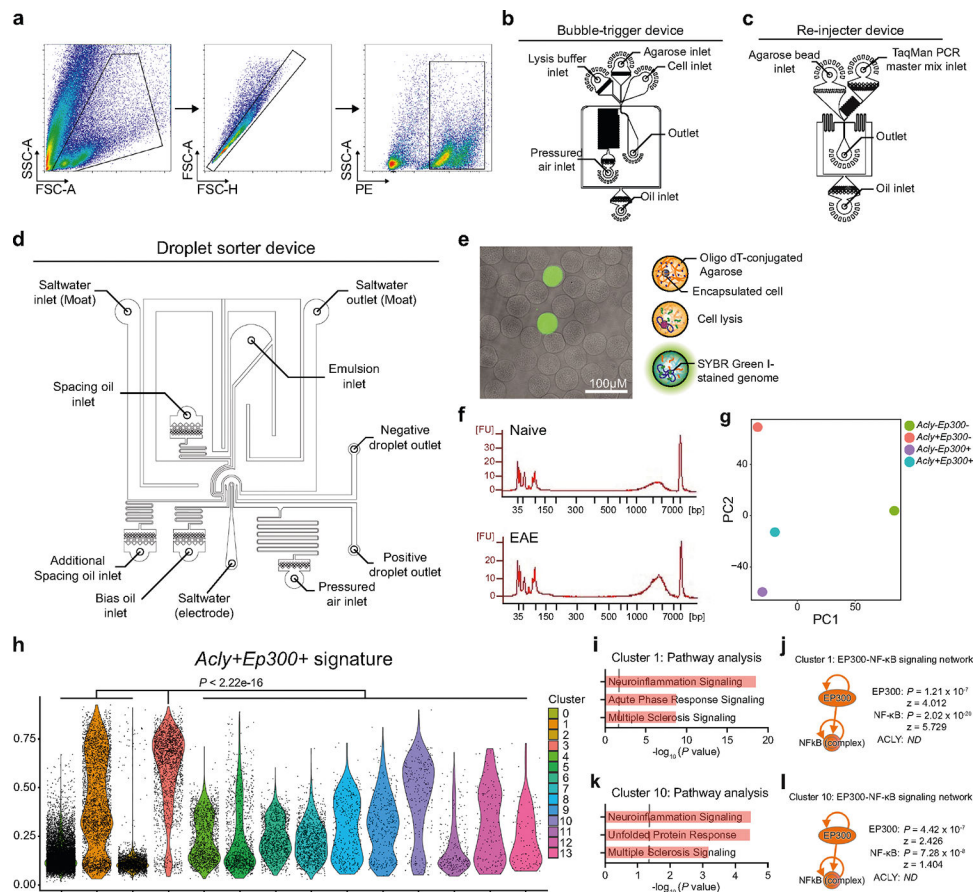
(a) Experimental design for (c). (b) NOD EAE score for (c) ($n = 3$ per group). (c) Naïve and EAE induced NOD mice received ICV administration of IL-1 β /TNF (EAE progressive, Day 124). After 18–24 h, sorted brain astrocytes were analyzed by qPCR ($n = 3$ per group). Unpaired two-sided t -test. (d) Immunostaining (left) and quantification (right) of H3K27ac⁺ and p300⁺ astrocytes in mice with/without NOD EAE ($n = 9$ spinal cord sections; $n = 3$ mice per group). Astrocyte H3K27ac levels were calculated as the mean signal intensity (arbitrary units) per GFAP⁺ cells using automated unbiased quantification. Unpaired two-sided t -test. (e) Immunostaining (left) and quantification (right) of ACLY⁺, p300⁺, and ACLY⁺p300⁺ astrocytes in mice with/without NOD EAE ($n = 9$ spinal cord sections; $n = 3$ mice per group). Unpaired two-sided t -test. (f) NOD EAE curves (*sgScrmbl*; $n = 7$; *sgEp300*; $n = 8$; *sgAcly*; $n = 7$). Lentivirus were injected at day 40. Representative data of two independent experiments. Regression slope two-sided t -test compared with *sgScrmbl*. (g) Volcano plot of differential gene expression determined by RNA-seq in astrocytes isolated from *sgScrmbl*-, *sgEp300*-, and *sgAcly*-transduced mice 64 days after NOD EAE induction ($n = 3$ *sgScrmbl*, $n = 3$ *sgEp300*, $n = 2$ *sgAcly*). (h) GSEA analysis comparing *sgScrmbl*-, *sgEp300*-, and *sgAcly*-transduced astrocytes. (i) Staining with FluoroMyelin dye and percentage of myelin loss from *sgScrmbl*-, *sgEp300*-, and *sgAcly*-transduced mice spinal cord ($n = 6$ spinal cord

sections (*sgEp300*); n = 9 spinal cord sections (*sgScrmbl*, *sgAcly*); n = 3 mice per group. Lesions indicated by arrowheads. Unpaired two-sided *t*-test. Data shown as mean ± s.e.m.



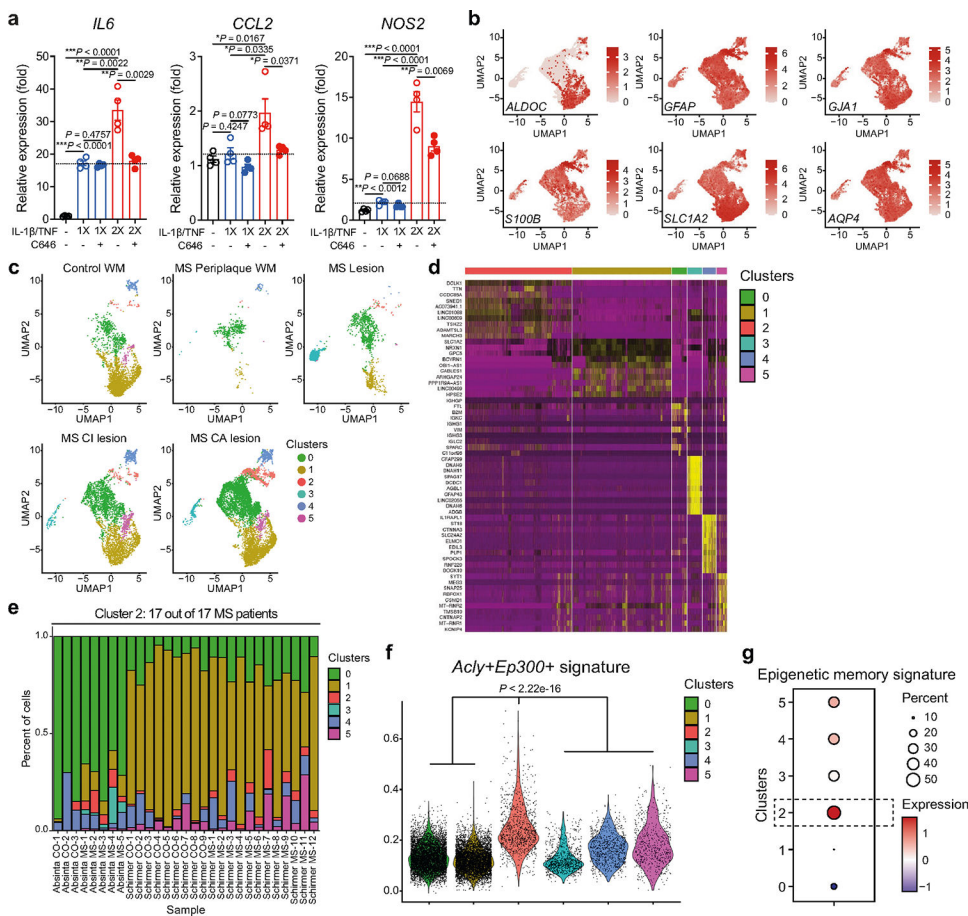
Extended Data Fig. 7 | ACLY and p300 signaling in NOD EAE astrocytes.

(a) Immunostaining (left) and quantification (right) of H3K27ac⁺ and p300⁺ astrocytes from *sgScrmbl*- and *sgEp300*-transduced NOD mice 64 days after EAE induction (n = 6 spinal cord sections; n = 3 mice per group). Unpaired two-sided *t*-test. **(b)** Immunostaining (left) and quantification (right) of H3K27ac⁺ and ACLY⁺ astrocytes from *sgScrmbl*- and *sgAcly*-transduced NOD mice 64 days after EAE induction (n = 6 spinal cord sections; n = 3 mice per group). Unpaired two-sided *t*-test. **(c)** Quantification of CNS-resident cells from *sgScrmbl*-, *sgEp300*-, and *sgAcly*-transduced mice (n = 7 per group). Unpaired two-sided *t*-test. **(d,e)** Analysis of CNS T cells (up) and splenic T cells (bottom) from *sgScrmbl*-, *sgEp300*-, and *sgAcly*-transduced mice (n = 4 per group). Unpaired two-sided *t*-test. Data shown as mean ± s.e.m.



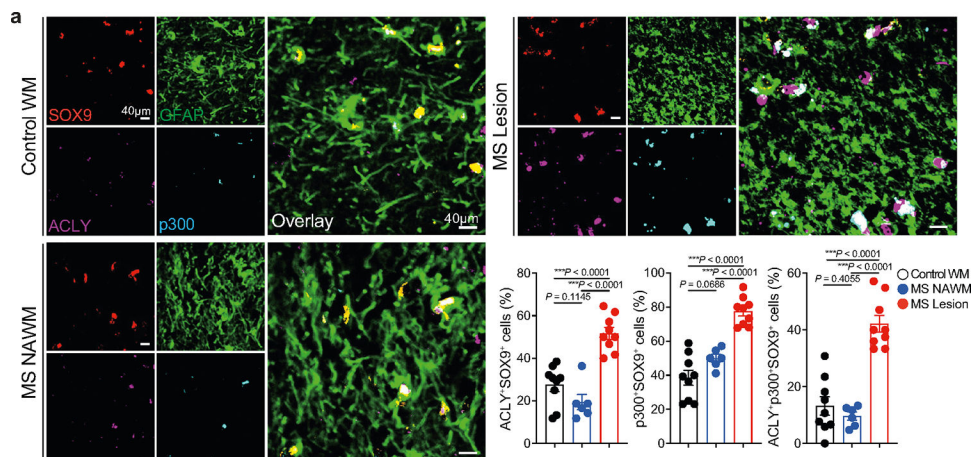
Extended Data Fig. 8 | Analysis of *AclY*⁺*Ep300*⁺ astrocytes by FIND-seq.

(a) FACS sorting schematic for tdTomato^{Gfap} astrocytes. **(b-d)** Schematic illustration of microfluidic devices utilized in FIND-seq. **(b)** The bubble-triggered device has with five inlets: i) cell inlet, ii) Oligo dT primer-conjugated agarose inlet, iii) lysis buffer inlet, iv) oil inlet, and v) pressurized air inlet. **(c)** The re-injector device has three inlets: i) agarose bead inlet, ii) TaqMan PCR master mix inlet, and iii) oil inlet. **(d)** The droplet sorter device has seven inlets: i) emulsion inlet, ii) spacing oil inlet, iii) additional spacing oil inlet, iv) bias oil inlet, v) saltwater inlet (for the electrode), vi) saltwater inlet (for the moat), and vii) pressurized air inlet. **(e)** Astrocytes are encapsulated in an agarose bead along with the lysis buffer. The genome entrapped in the agarose bead is stained with SYBR Green I and visualized using a fluorescence microscope. **(f)** cDNA, produced on the agarose bead, is amplified via WTA and validated using a Bioanalyzer. **(g)** Principal component analysis (PCA) plot of *AclY*⁻*Ep300*⁻, *AclY*⁺*Ep300*⁻, *AclY*⁻*Ep300*⁺, *AclY*⁺*Ep300*⁺ EAE astrocytes. **(h)** Violin plot depicting *AclY*⁺*Ep300*⁺ EAE astrocyte signature expression in EAE astrocytes. **(i)** IPA pathway analysis up-regulated (red) in cluster 1 astrocytes. **(j)** EP300-NF-κB signaling network of cluster 1 astrocytes. **(k)** IPA pathway analysis up-regulated (red) in cluster 10 astrocytes. **(l)** EP300-NF-κB signaling network of cluster 10 astrocytes.



Extended Data Fig. 9 | Analysis of human astrocyte epigenetic memory and MS astrocyte scRNA-seq.

(a) Primary human fetal astrocytes received IL-1 β /TNF stimulation once (1X) or twice (2X). qPCR of astrocytes in the presence with/without C646 (p300/CBP inhibitor) after 2 h stimulation with IL-1 β /TNF on day 7 (n = 4 per group). Unpaired two-sided *t*-test. (b) Gene scatterplots of astrocyte markers. (c) Unsupervised clustering UMAP plot of astrocytes from patients with MS and control individuals from Schirmer et al.³¹ and Absinta et al.³⁰. (n = 16,276 cells). WM, white matter; CI, chronic inactive; CA, chronic active. (d) Significantly enriched genes by astrocyte cell type cluster. (e) Cluster distribution of CNS cells. (f) Violin plot depicting *Acly*⁺*Ep300*⁺ EAE astrocyte signature expression in MS astrocytes. (g) Astrocyte epigenetic memory signature score in astrocyte clusters of control and MS patients.



Extended Data Fig. 10 | ACLY + p300+ astrocytes in MS patients.

(a) Immunostaining and quantification of ACLY⁺SOX9⁺, p300⁺SOX9⁺, ACLY⁺p300⁺SOX9⁺ astrocytes in CNS samples from MS patients with MS (n = 9 sections (Lesion); n = 6 sections (NAWM); n = 3 per patient) and controls (n = 3 sections; n = 3 per patient). WM, white matter; NAWM, normally appearing white matter. Unpaired two-sided *t*-test. Data shown as mean ± s.e.m.

Supplementary Material

Refer to Web version on PubMed Central for supplementary material.

Acknowledgements

This work was supported by grants NS102807, ES02530, ES029136, AI126880 from the NIH; RG4111A1 and JF2161-A-5 from the NMSS; RSG-14-198-01-LIB from the American Cancer Society; and PA-1604-08459 from the International Progressive MS Alliance. H.-G.L. was supported by a Basic Science Research Program through the National Research Foundation of Korea (NRF) funded by the Ministry of Education (2021R1A6A3A14039088). J.-H.L. was supported by the Basic Science Research Program funded by the National Research Foundation of Korea (NRF)/Ministry of Education (2022R1A6A3A03071157) and a long-term postdoctoral fellowship funded by the Human Frontier Science Program (LT0015/2023-L). T.I. was supported by the EMBO postdoctoral fellowship (ALTF: 1009–2021). G.P. is a trainee in the Medical Scientist Training Program funded by NIH T32 GM007356. The content of this manuscript is solely the responsibility of the authors and does not necessarily represent the official views of the National Institute of General Medical Science or NIH. M.A.W. was supported by NINDS, NIMH and NCI (R01MH132632, R01MH130458, R00NS114111, T32CA207201). A.P. holds the T1 Canada Research Chair in MS and is funded by the Canada Institute of Health Research, the NMSS and the Canadian Foundation for Innovation. I.C.C. was supported by K22AI152644 and DP2AI154435 from the NIH. The authors thank L. Li for technical assistance; all members of the Quintana laboratory for helpful advice and discussions; R. Krishnan for technical assistance with flow cytometry; and BDRL members K. A. Aldinger, D. Doherty, I. G. Phelps, J. C. Dempsey, K. J. Lee and L. A. Cort.

Data availability

Sequencing data were deposited into GEO under the SuperSeries accession numbers GSE252551, GSE237558 and GSE252498. Source data are provided with this paper.

References

1. Rothhammer V et al. Type I interferons and microbial metabolites of tryptophan modulate astrocyte activity and central nervous system inflammation via the aryl hydrocarbon receptor. *Nat. Med.* 22, 586–597 (2016). [PubMed: 27158906]

2. Wheeler MA et al. MAFG-driven astrocytes promote CNS inflammation. *Nature* 578, 593–599 (2020). [PubMed: 32051591]
3. Sanmarco LM et al. Gut-licensed IFN γ ⁺ NK cells drive LAMP1⁺TRAIL⁺ anti-inflammatory astrocytes. *Nature* 590, 473–479 (2021). [PubMed: 33408417]
4. Wheeler MA et al. Environmental control of astrocyte pathogenic activities in CNS inflammation. *Cell* 176, 581–596.e518 (2019). [PubMed: 30661753]
5. Wheeler MA et al. Droplet-based forward genetic screening of astrocyte-microglia cross-talk. *Science* 379, 1023–1030 (2023). [PubMed: 36893254]
6. Clark IC et al. Barcoded viral tracing of single-cell interactions in central nervous system inflammation. *Science* 372, eabf1230 (2021). [PubMed: 33888612]
7. Rothhammer V et al. Microglial control of astrocytes in response to microbial metabolites. *Nature* 557, 724–728 (2018). [PubMed: 29769726]
8. Chao CC et al. Metabolic control of astrocyte pathogenic activity via cPLA2-MAVS. *Cell* 179, 1483–1498.e1422 (2019). [PubMed: 31813625]
9. Allen NJ & Lyons DA Glia as architects of central nervous system formation and function. *Science* 362, 181–185 (2018). [PubMed: 30309945]
10. Lee HG, Wheeler MA & Quintana FJ Function and therapeutic value of astrocytes in neurological diseases. *Nat. Rev. Drug Discov.* 21, 339–358 (2022). [PubMed: 35173313]
11. Sofroniew MV Astrocyte barriers to neurotoxic inflammation. *Nat. Rev. Neurosci.* 16, 249–263 (2015). [PubMed: 25891508]
12. Yu X & Khakh BS SnapShot: astrocyte interactions. *Cell* 185, 220–220.e221 (2022). [PubMed: 34995516]
13. Lee HG, Lee JH, Flausino LE & Quintana FJ Neuroinflammation: an astrocyte perspective. *Sci. Transl. Med.* 15, eadi7828 (2023). [PubMed: 37939162]
14. Liddelow SA et al. Neurotoxic reactive astrocytes are induced by activated microglia. *Nature* 541, 481–487 (2017). [PubMed: 28099414]
15. Endo F et al. Molecular basis of astrocyte diversity and morphology across the CNS in health and disease. *Science* 378, eadc9020 (2022). [PubMed: 36378959]
16. Habib N et al. Disease-associated astrocytes in Alzheimer’s disease and aging. *Nat. Neurosci.* 23, 701–706 (2020).
17. Zinkernagel RM et al. On immunological memory. *Annu. Rev. Immunol.* 14, 333–367 (1996). [PubMed: 8717518]
18. Wendeln AC et al. Innate immune memory in the brain shapes neurological disease hallmarks. *Nature* 556, 332–338 (2018). [PubMed: 29643512]
19. Saeed S et al. Epigenetic programming of monocyte-to-macrophage differentiation and trained innate immunity. *Science* 345, 1251086 (2014). [PubMed: 25258085]
20. Sun JC, Beilke JN & Lanier LL Adaptive immune features of natural killer cells. *Nature* 457, 557–561 (2009). [PubMed: 19136945]
21. Serafini N et al. Trained ILC3 responses promote intestinal defense. *Science* 375, 859–863 (2022). [PubMed: 35201883]
22. Netea MG et al. Defining trained immunity and its role in health and disease. *Nat. Rev. Immunol.* 20, 375–388 (2020). [PubMed: 32132681]
23. Perkins ND et al. Regulation of NF- κ B by cyclin-dependent kinases associated with the p300 coactivator. *Science* 275, 523–527 (1997). [PubMed: 8999795]
24. Zhao J, Li X, Guo M, Yu J & Yan C The common stress responsive transcription factor ATF3 binds genomic sites enriched with p300 and H3K27ac for transcriptional regulation. *BMC Genomics* 17, 335 (2016). [PubMed: 27146783]
25. Magistretti PJ & Allaman I Lactate in the brain: from metabolic end-product to signalling molecule. *Nat. Rev. Neurosci.* 19, 235–249 (2018). [PubMed: 29515192]
26. Pietrocola F, Galluzzi L, Bravo-San Pedro JM, Madeo F & Kroemer G Acetyl coenzyme A: a central metabolite and second messenger. *Cell Metab.* 21, 805–821 (2015). [PubMed: 26039447]
27. Wellen KE et al. ATP-citrate lyase links cellular metabolism to histone acetylation. *Science* 324, 1076–1080 (2009). [PubMed: 19461003]

28. Mayo L et al. Regulation of astrocyte activation by glycolipids drives chronic CNS inflammation. *Nat. Med.* 20, 1147–1156 (2014). [PubMed: 25216636]
29. Cla C, et al. Identification of astrocyte regulators by nucleic acid cytometry. *Nature* 614, 326–333 (2023). [PubMed: 36599367]
30. Absinta M et al. A lymphocyte-microglia-astrocyte axis in chronic active multiple sclerosis. *Nature* 597, 709–714 (2021). [PubMed: 34497421]
31. Schirmer L et al. Neuronal vulnerability and multilineage diversity in multiple sclerosis. *Nature* 573, 75–82 (2019). [PubMed: 31316211]
32. Cheong JG et al. Epigenetic memory of coronavirus infection in innate immune cells and their progenitors. *Cell* 186, 3882–3902.e3824 (2023). [PubMed: 37597510]
33. Yao Y et al. Induction of autonomous memory alveolar macrophages requires T cell help and is critical to trained immunity. *Cell* 175, 1634–1650.e1617 (2018). [PubMed: 30433869]
34. McCarthy GF & Leblond CP Radioautographic evidence for slow astrocyte turnover and modest oligodendrocyte production in the corpus callosum of adult mice infused with ³H-thymidine. *J. Comp. Neurol.* 271, 589–603 (1988). [PubMed: 3385018]
35. Chierzi S et al. Astrocytes transplanted during early postnatal development integrate, mature, and survive long term in mouse cortex. *J. Neurosci.* 43, 1509–1529 (2023). [PubMed: 36669885]
36. Ogryzko VV, Schiltz RL, Russanova V, Howard BH & Nakatani Y The transcriptional coactivators p300 and CBP are histone acetyltransferases. *Cell* 87, 953–959 (1996). [PubMed: 8945521]
37. Li Q, Xiao H & Isobe K Histone acetyltransferase activities of cAMP-regulated enhancer-binding protein and p300 in tissues of fetal, young, and old mice. *J. Gerontol. A* 57, B93–B98 (2002).
38. Farrelly LA et al. Histone serotonylation is a permissive modification that enhances TFIID binding to H3K4me3. *Nature* 567, 535–539 (2019). [PubMed: 30867594]
39. Lepack AE et al. Dopaminylation of histone H3 in ventral tegmental area regulates cocaine seeking. *Science* 368, 197–201 (2020). [PubMed: 32273471]
40. Mews P et al. Acetyl-CoA synthetase regulates histone acetylation and hippocampal memory. *Nature* 546, 381–386 (2017). [PubMed: 28562591]
41. Sen P et al. Histone acetyltransferase p300 induces de novo super-enhancers to drive cellular senescence. *Mol. Cell* 73, 684–698.e688 (2019). [PubMed: 30773298]
42. Furman D et al. Chronic inflammation in the etiology of disease across the life span. *Nat. Med.* 25, 1822–1832 (2019). [PubMed: 31806905]
43. Li TY et al. The transcriptional coactivator CBP/p300 is an evolutionarily conserved node that promotes longevity in response to mitochondrial stress. *Nat Aging* 1, 165–178 (2021). [PubMed: 33718883]
44. Burda JE et al. Divergent transcriptional regulation of astrocyte reactivity across disorders. *Nature* 606, 557–564 (2022). [PubMed: 35614216]
45. Chen L, Fischle W, Verdin E & Greene WC Duration of nuclear NF- κ B action regulated by reversible acetylation. *Science* 293, 1653–1657 (2001). [PubMed: 11533489]
46. Long L et al. CRISPR screens unveil signal hubs for nutrient licensing of T cell immunity. *Nature* 600, 308–313 (2021). [PubMed: 34795452]
47. Beigneux AP et al. ATP-citrate lyase deficiency in the mouse. *J. Biol. Chem.* 279, 9557–9564 (2004). [PubMed: 14662765]
48. Hochrein SM et al. The glucose transporter GLUT3 controls T helper 17 cell responses through glycolytic-epigenetic reprogramming. *Cell Metab.* 34, 516–532. e511 (2022). [PubMed: 35316657]
49. Balmer ML et al. Memory CD8⁺ T cells require increased concentrations of acetate induced by stress for optimal function. *Immunity* 44, 1312–1324 (2016). [PubMed: 27212436]
50. Lauterbach MA et al. Toll-like receptor signaling rewires macrophage metabolism and promotes histone acetylation via ATP-citrate lyase. *Immunity* 51, 997–1011.e1017 (2019). [PubMed: 31851905]
51. Sardar D et al. Induction of astrocytic Slc22a3 regulates sensory processing through histone serotonylation. *Science* 380, eade0027 (2023). [PubMed: 37319217]

52. Krausgruber T et al. Structural cells are key regulators of organ-specific immune responses. *Nature* 583, 296–302 (2020). [PubMed: 32612232]
53. Hatzivassiliou G et al. ATP citrate lyase inhibition can suppress tumor cell growth. *Cancer Cell* 8, 311–321 (2005). [PubMed: 16226706]
54. Verschuere KHG et al. Structure of ATP citrate lyase and the origin of citrate synthase in the Krebs cycle. *Nature* 568, 571–575 (2019). [PubMed: 30944476]
55. Wei J et al. An allosteric mechanism for potent inhibition of human ATP-citrate lyase. *Nature* 568, 566–570 (2019). [PubMed: 30944472]
56. Garcia AD, Doan NB, Imura T, Bush TG & Sofroniew MV GFAP-expressing progenitors are the principal source of constitutive neurogenesis in adult mouse forebrain. *Nat. Neurosci.* 7, 1233–1241 (2004). [PubMed: 15494728]
57. Madisen L et al. A robust and high-throughput Cre reporting and characterization system for the whole mouse brain. *Nat. Neurosci.* 13, 133–140 (2010). [PubMed: 20023653]
58. Everhart MB et al. Duration and intensity of NF- κ B activity determine the severity of endotoxin-induced acute lung injury. *J. Immunol.* 176, 4995–5005 (2006). [PubMed: 16585596]
59. Gutierrez-Vazquez C & Quintana FJ Protocol for in vitro analysis of pro-inflammatory and metabolic functions of cultured primary murine astrocytes. *STAR Protoc.* 3, 101033 (2022). [PubMed: 34977679]
60. Thompson AJ et al. Diagnosis of multiple sclerosis: 2017 revisions of the McDonald criteria. *Lancet Neurol.* 17, 162–173 (2018). [PubMed: 29275977]
61. Dhazee T et al. CD70 defines a subset of proinflammatory and CNS-pathogenic T_H1/T_H17 lymphocytes and is overexpressed in multiple sclerosis. *Cell Mol. Immunol.* 16, 652–665 (2019). [PubMed: 30635649]
62. Broux B et al. Interleukin-26, preferentially produced by TH17 lymphocytes, regulates CNS barrier function. *Neurol. Neuroimmunol. Neuroinflamm.* 7, e870 (2020). [PubMed: 32788322]
63. Illouz T, Madar R, Hirsh T, Biragyn A & Okun E Induction of an effective anti-amyloid- β humoral response in aged mice. *Vaccine* 39, 4817–4829 (2021). [PubMed: 34294479]
64. Illouz T et al. Maternal antibodies facilitate amyloid- β clearance by activating Fc-receptor–Syk-mediated phagocytosis. *Commun. Biol.* 4, 329 (2021). [PubMed: 33712740]
65. Motulsky HJ & Brown RE Detecting outliers when fitting data with nonlinear regression—a new method based on robust nonlinear regression and the false discovery rate. *BMC Bioinformatics* 7, 123 (2006). [PubMed: 16526949]
66. Sanjana NE, Shalem O & Zhang F Improved vectors and genome-wide libraries for CRISPR screening. *Nat. Methods* 11, 783–784 (2014). [PubMed: 25075903]
67. Chen S et al. Genome-wide CRISPR screen in a mouse model of tumor growth and metastasis. *Cell* 160, 1246–1260 (2015). [PubMed: 25748654]
68. Lee Y, Messing A, Su M & Brenner M GFAP promoter elements required for region-specific and astrocyte-specific expression. *Glia* 56, 481–493 (2008). [PubMed: 18240313]
69. Wang T et al. Gene essentiality profiling reveals gene networks and synthetic lethal interactions with oncogenic Ras. *Cell* 168, 890–903.e815 (2017). [PubMed: 28162770]
70. Foo LC Purification of rat and mouse astrocytes by immunopanning. *Cold Spring Harb. Protoc.* 2013, 421–432 (2013). [PubMed: 23637363]
71. Lemaitre F et al. Capturing T lymphocytes’ dynamic interactions with human neural cells using time-lapse microscopy. *Front. Immunol.* 12, 668483 (2021). [PubMed: 33968073]
72. Durafourt BA, Moore CS, Blain M & Antel JP Isolating, culturing, and polarizing primary human adult and fetal microglia. *Methods Mol. Biol.* 1041, 199–211 (2013). [PubMed: 23813381]
73. Kieran NW et al. MicroRNA-210 regulates the metabolic and inflammatory status of primary human astrocytes. *J. Neuroinflammation* 19, 10 (2022). [PubMed: 34991629]
74. van Galen P et al. A multiplexed system for quantitative comparisons of chromatin landscapes. *Mol. Cell* 61, 170–180 (2016). [PubMed: 26687680]
75. Untergasser A et al. Primer3—new capabilities and interfaces. *Nucleic Acids Res.* 40, e115 (2012). [PubMed: 22730293]

76. Trombetta JJ et al. Preparation of single-cell RNA-seq libraries for next generation sequencing. *Curr. Protoc. Mol. Biol.* 107, 4.22.1–4.22.17 (2014).
77. Langmead B & Salzberg SL Fast gapped-read alignment with Bowtie 2. *Nat. Methods* 9, 357–359 (2012). [PubMed: 22388286]
78. Tarasov A, Vilella AJ, Cuppen E, Nijman IJ & Prins P Sambamba: fast processing of NGS alignment formats. *Bioinformatics* 31, 2032–2034 (2015). [PubMed: 25697820]
79. Li H et al. The Sequence Alignment/Map format and SAMtools. *Bioinformatics* 25, 2078–2079 (2009). [PubMed: 19505943]
80. Ramirez F, Dundar F, Diehl S, Gruning BA & Manke T deepTools: a flexible platform for exploring deep-sequencing data. *Nucleic Acids Res.* 42, W187–191 (2014). [PubMed: 24799436]
81. Zhang Y et al. Model-based analysis of ChIP-seq (MACS). *Genome Biol.* 9, R137 (2008). [PubMed: 18798982]
82. Buenrostro JD, Giresi PG, Zaba LC, Chang HY & Greenleaf WJ Transposition of native chromatin for fast and sensitive epigenomic profiling of open chromatin, DNA-binding proteins and nucleosome position. *Nat. Methods* 10, 1213–1218 (2013). [PubMed: 24097267]
83. Buenrostro JD, Wu B, Chang HY & Greenleaf WJ ATAC-seq: a method for assaying chromatin accessibility genome-wide. *Curr. Protoc. Mol. Biol.* 109, 21.29.21–21.29.29 (2015).
84. Clark IC, Thakur R & Abate AR Concentric electrodes improve microfluidic droplet sorting. *Lab Chip* 18, 710–713 (2018). [PubMed: 29383336]
85. Subramanian A et al. Gene set enrichment analysis: a knowledge-based approach for interpreting genome-wide expression profiles. *Proc. Natl Acad. Sci. USA* 102, 15545–15550 (2005). [PubMed: 16199517]
86. Mootha VK et al. PGC-1 α -responsive genes involved in oxidative phosphorylation are coordinately downregulated in human diabetes. *Nat. Genet.* 34, 267–273 (2003). [PubMed: 12808457]

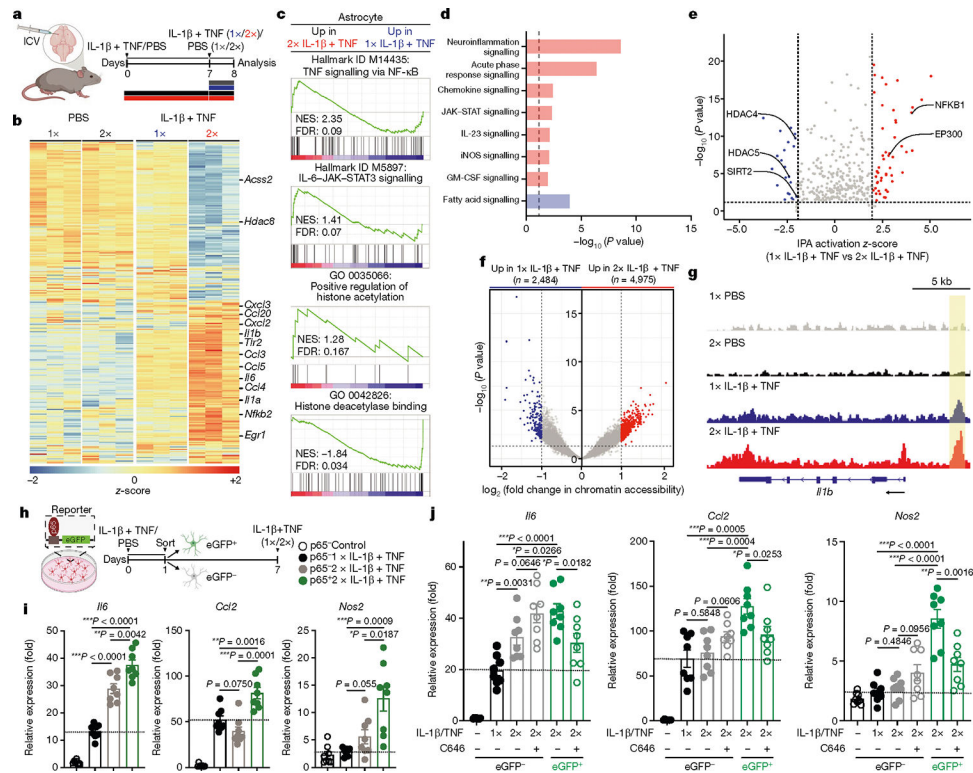


Fig. 1 | Pro-inflammatory stimuli induce astrocyte epigenetic memory.

a, Experimental design for **b–g**. C57BL/6 mice received ICV administration of IL-1 β and TNF or PBS once (1 \times) or twice (2 \times). After 18 h, sorted brain astrocytes were analysed. **b**, Differential gene expression determined by RNA-seq in sorted astrocytes ($n = 3$ per group). **c**, Gene set enrichment analysis (GSEA) comparing astrocytes stimulated twice (2 \times) versus once (1 \times). Gene Ontology (GO) terms are shown. FDR, false discovery rate; NES, normalized enrichment score. **d,e**, IPA (**d**) and predicted upstream regulators (**e**) in isolated astrocytes. Up-regulated (red) or down-regulated (blue) genes in astrocytes stimulated twice (2 \times) versus once (1 \times) are shown. **f,g**, ATAC-seq analysis of astrocytes comparing 2 \times IL-1 β + TNF versus 1 \times IL-1 β + TNF ($n = 5$ per group). **f**, Genes with increased (red) or decreased (blue) accessibility in astrocytes. **g**, Genome browser snapshots showing ATAC-seq sequencing tracks at the *Il1b* locus. Regions with a significant increase ($P < 0.05$) in accessibility in astrocytes from mice stimulated twice (2 \times) versus once (1 \times) are indicated by the yellow band. **h**, Experimental design for **i**. Primary astrocytes isolated from *p65*-eGFP reporter mice received PBS or IL-1 β + TNF stimulation. After 18–24 h, eGFP-positive and negative astrocytes were sorted and received IL-1 β + TNF stimulation once (1 \times) or twice (2 \times) after 6 days. **i**, Quantitative PCR (qPCR) of eGFP-positive and negative astrocytes after 30 min stimulation with IL-1 β + TNF on day 7 ($n = 8$ per group). Unpaired two-sided *t*-test. **j**, Gene expression 30 min after IL-1 β + TNF stimulation on day 7 of eGFP-positive and negative astrocytes treated with C646 or vehicle ($n = 8$ per group). Unpaired two-sided *t*-test. Data are mean \pm s.e.m. Dotted lines indicate significance ($P < 0.05$).

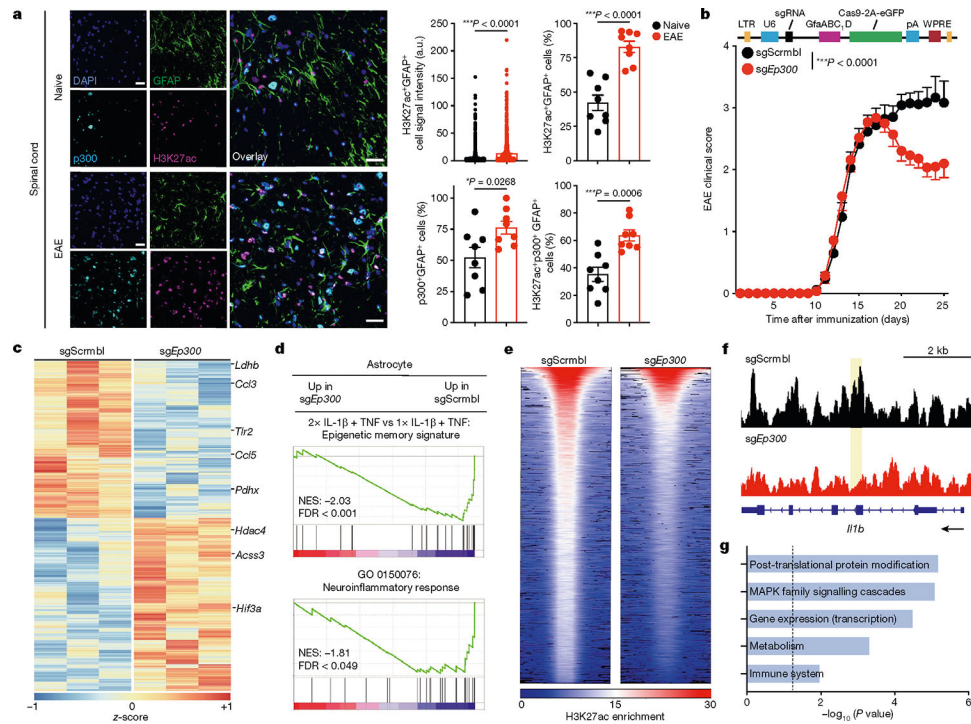


Fig. 2 | p300 promotes astrocyte epigenetic memory in EAE.

a, Immunostaining (left) and quantification (right) of H3K27ac⁺ and p300⁺ astrocytes in mice with or without EAE ($n = 8$ spinal cord sections; $n = 3$ mice per group). Astrocyte H3K27ac levels were calculated as the mean signal intensity (arbitrary units) per GFAP⁺ cell using automated unbiased quantification. Unpaired two-sided t -test. Scale bars, 25 μ m. **b**, EAE curves in mice treated with non-targeting single guide RNA (sgScrmbl) ($n = 17$) or single guide RNA (sgRNA) targeting *Ep300* (sgEp300) ($n = 14$) mice. Representative data of three independent experiments. Two-way repeated measures of ANOVA. **c**, Differential gene expression determined by RNA-seq in astrocytes from sgScrmbl- and sgEp300-transduced mice 23 days after EAE induction ($n = 3$ per group). **d**, GSEA comparing sgScrmbl- and sgEp300-transduced astrocytes. **e,f**, ChIP-seq analysis of sgScrmbl- and sgEp300-transduced astrocytes ($n = 3$ per group). **e**, Heat map showing dynamic H3K27 acetylation marks. **f**, Genome browser snapshots showing the *Il1b* locus. Regions showing a significant decrease ($P < 0.05$) in accessibility in sgScrmbl-transduced versus sgEp300-transduced astrocytes are highlighted by the yellow band. **g**, Reactome pathway analysis showing down-regulated ChIP-seq-accessible peaks of isolated astrocytes comparing sgScrmbl-transduced versus sgEp300-transduced astrocytes. Dotted line indicates significance ($P < 0.05$). Data are mean \pm s.e.m. LTR, long terminal repeat; pA, polyA; U6, promoter; WRPE, woodchuck hepatitis virus post-transcriptional regulatory element.

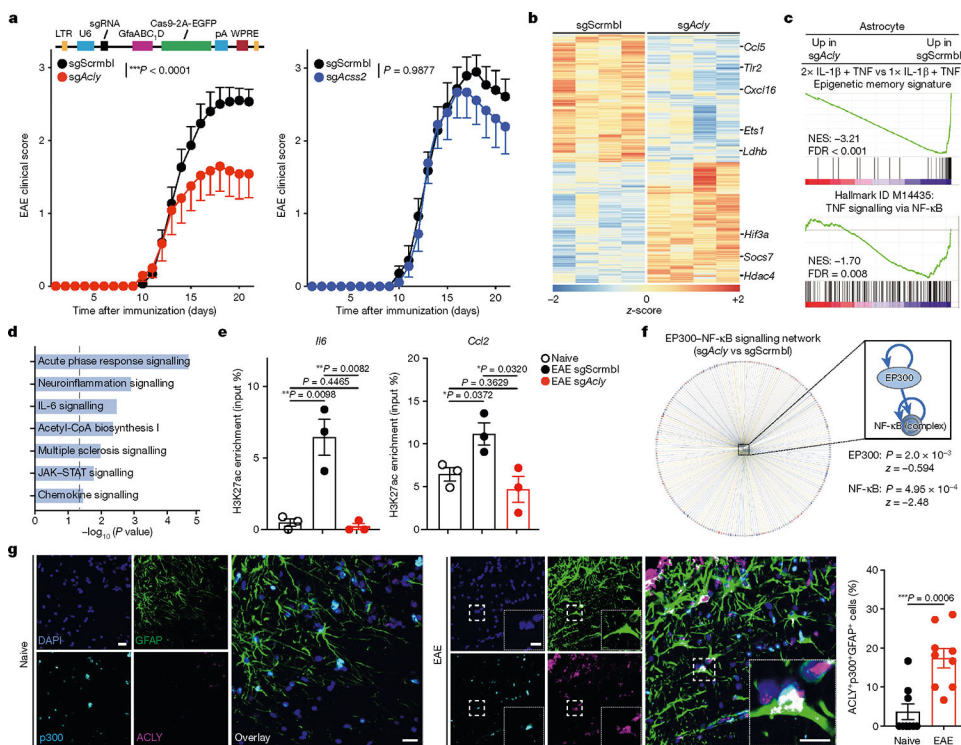


Fig. 3 | ACLY controls p300-derived astrocyte epigenetic memory in EAE.

a, EAE curves. Left: sgScrmbl, $n = 15$; *Acly*-targeting sgRNA (*sgAcly*), $n = 12$. Right: sgScrmbl, $n = 14$; *sgAcss2*, $n = 9$. Representative data of at least two independent experiments. Two-way repeated measures of ANOVA. **b**, Differential gene expression determined by RNA-seq in astrocytes from sgScrmbl- and *sgAcly*-transduced mice 21 days after EAE induction ($n = 4$ per group). **c**, GSEA analysis comparing sgScrmbl- and *sgAcly*-transduced astrocytes. **d**, IPA showing down-regulated genes in *sgAcly*-versus sgScrmbl-transduced astrocytes. **e**, Chromatin immunoprecipitation with qPCR analysis of the abundance of H3K27ac in pro-inflammatory gene promoters, comparing sgScrmbl- and *sgAcly*-transduced astrocytes ($n = 3$ per group). Unpaired two-sided t -test. Dotted line indicates significance ($P < 0.05$). **f**, Analysis of the EP300–NF- κ B signalling network, comparing sgScrmbl- and *sgAcly*-transduced astrocytes. **g**, Immunostaining (left; scale bars, 20 μ m, middle; scale bars, 10 μ m) and quantification (right) of ACLY⁺p300⁺ astrocytes in mice with or without EAE ($n = 9$ spinal cord sections; $n = 3$ mice per group). Unpaired two-sided t -test. Data are mean \pm s.e.m.

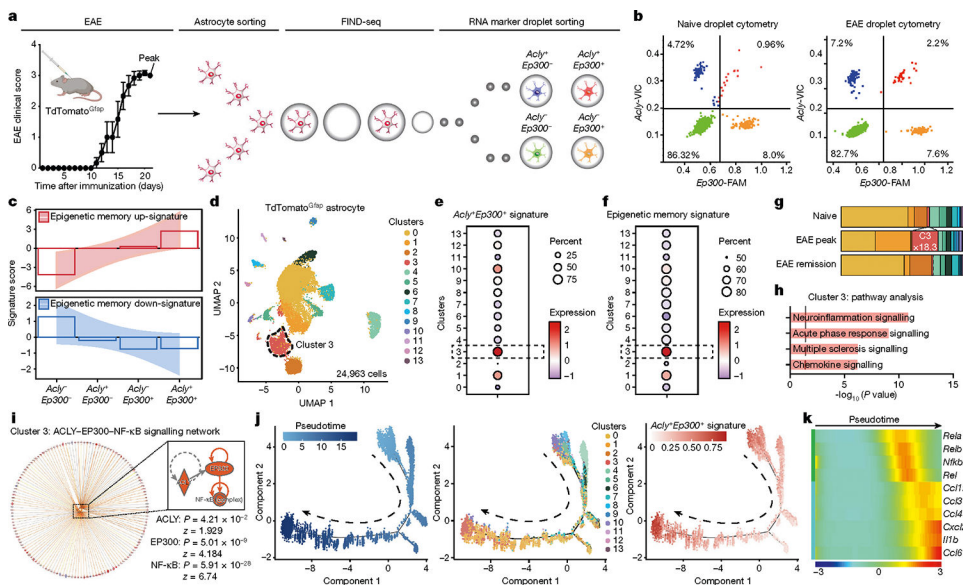


Fig. 4 |. Analysis of *Acly*⁺*Ep300*⁺ astrocytes with FIND-seq.

a, TdTomato^{Gfap} astrocytes from naive and EAE mice were pooled ($n = 3$ per group) and analysed by FIND-seq using *Acly* and *Ep300* expression. EAE curve ($n = 3$ per group). Two-way repeated measures of ANOVA. **b**, Representative droplet cytometry plots. Numbers in each quadrant display the percentage of astrocytes in droplets. **c**, Astrocyte epigenetic memory signature score in *Acly*⁻*Ep300*⁻, *Acly*⁺*Ep300*⁻, *Acly*⁻*Ep300*⁺ and *Acly*⁺*Ep300*⁺ EAE astrocytes. **d**, Uniform manifold approximation and projection (UMAP) plot of TdTomato^{Gfap} astrocytes² ($n = 24,963$ cells). **e**, *Acly*⁺*Ep300*⁺ EAE astrocyte signature expression in EAE astrocyte clusters. **f**, Astrocyte epigenetic memory signature score in EAE astrocyte clusters. **g**, Fraction of cells per cluster overall. **h**, IPA up-regulated pathways (red) in cluster 3 astrocytes. **i**, ACly-EP300-NF-κB signalling network of cluster 3 astrocytes. **j**, Pseudotime trajectory in TdTomato^{Gfap} astrocytes. Each cell is coloured to indicate its pseudotime value. **k**, Pseudotime analysis of gene expression in TdTomato^{Gfap} astrocytes.

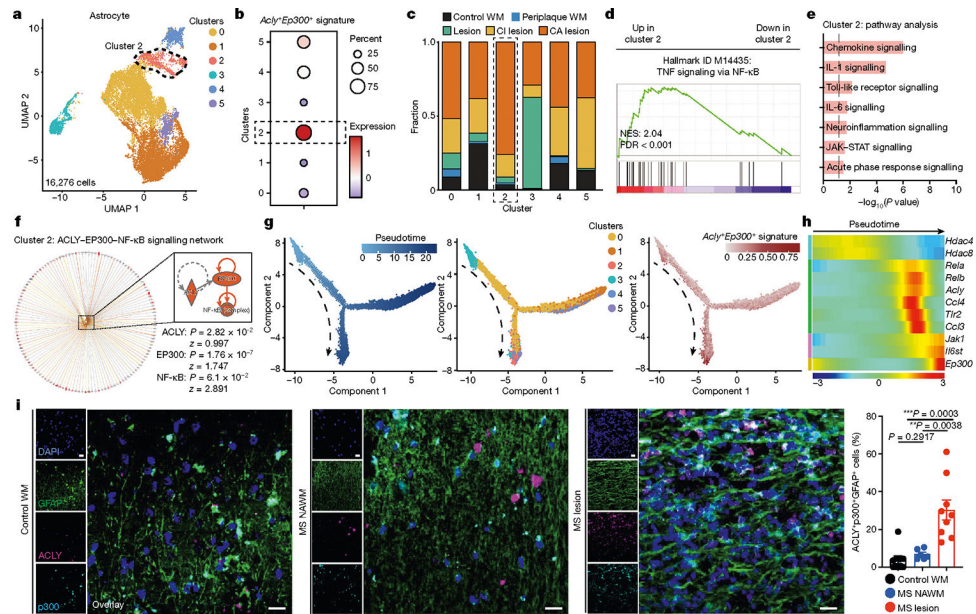


Fig. 5 | Identification of astrocyte epigenetic memory in multiple sclerosis.

a, UMAP plot of astrocytes from patients with multiple sclerosis and control individuals from Schirmer et al.³¹ and Absinta et al.³⁰. $n = 16,276$ cells. **b**, *Acly*⁺ *Ep300*⁺ EAE astrocyte signature expression in multiple sclerosis astrocyte clusters. **c**, Cluster analysis of astrocytes based on percent composition in multiple sclerosis. WM, white matter; CI, chronic inactive; CA, chronic active. **d**, GSEA analysis of cluster 2 astrocytes. **e**, IPA showing up-regulated pathways in cluster 2 astrocytes. **f**, ACLY–EP300–NF- κ B signalling network of cluster 2 astrocytes. **g**, Pseudotime trajectory in multiple sclerosis astrocytes. Each cell is coloured to indicate its pseudotime value. **h**, Pseudotime analysis of gene expression in multiple sclerosis astrocytes. **i**, Immunostaining and quantification of ACLY⁺, p300⁺ and ACLY⁺p300⁺ astrocytes in tissue samples from patients with multiple sclerosis ($n = 9$ sections (lesion); $n = 6$ sections (NAWM); $n = 3$ per patient) and control individuals ($n = 3$ sections; $n = 3$ per patient). NAWM, normally appearing white matter. Unpaired two-sided t -test. Data are mean \pm s.e.m. Scale bars, 20 μ m.